REPORT

# Recharge areas and geochemical evolution of groundwater in an alluvial aquifer system in the Sultanate of Oman

**Juerg M. Matter · H. N. Waber · S. Loew · A. Matter**

**Abstract** A regional hydrogeochemical model was developed to evaluate the geochemical evolution of different groundwaters in an alluvial aquifer system in the Interior of Oman. In combination with environmental isotopes the model is able to extract qualitative and quantitative information about recharge, groundwater flow paths and hydraulic connections between different aquifers. The main source of water to the alluvial aquifer along the flow paths of Wadi Abyadh and Wadi M'uaydin in the piedmont is groundwater from the high-altitude areas of the Jabal Akhdar and local infiltration along the wadi channels. In contrast, the piedmont alluvial aquifer along Wadi Halfayn is primarily replenished by lateral recharge from the ophiolite foothills to the east besides smaller contributions from the Jabal Akhdar and local infiltration. Further down gradient in the Southern Alluvial Plain aquifer a significant source of recharge is direct infiltration of rain and surface runoff, originating from a moisture source that approaches Oman from the south. The model shows that the main geochemical evolution of the alluvial groundwaters occurs along the flow path from the piedmont to the Southern Alluvial Plain, where dedolomitization is responsible for the observed changes in the chemical and carbon isotope composition in these waters.

Received: 30 September 2004 / Accepted: 9 December 2004
Published online: 8 September 2005



J. M. Matter (✉) · S. Loew
Geological Institute ETH Zuerich, Engineering Geology, ETH Hoenggerberg,
8093 Zuerich, Switzerland
e-mail: jmatter@ldeo.columbia.edu
Tel.: +1-845-365-8543
Fax: +1-845-365-8155

J. M. Matter
Present address: Lamont-Doherty Earth Observatory of Columbia University,
Geoscience 105B, 61 Route 9W, Palisades, NY, 10964 USA

H. N. Waber · A. Matter
Institute of Geological Sciences, University of Bern,
Baltzerstrasse 1,
3012 Bern, Switzerland

**Keywords** Arid regions · Groundwater flow · Groundwater recharge · Hydrochemical modeling · Stable isotopes

Résumé On a développé un modèle régional hydrogéochimique pour évaluer l'évolution géochimique des différentes eaux souterraines dans le système aquifère de l'intérieur d'Oman. Avec la contribution des isotopes d'environnement, le modèle est capable de fournir des informations qualitatives et quantitatives sur la recharge, les directions d'écoulement et sur les connections hydrauliques entre les différents aquifères du système. La source principale pour l'aquifère situé au long de la direction d'écoulement des oueds de Abdyah et de M'uaydin dans le piémont est l'eau souterraine provenant des zones de haute altitude de Jabal Akhbar ainsi que l'infiltration locale au long des canaux de l'oued. Par contre, à part d'une petite contribution provenant des infiltrations locaux et de Jabal Akhbar, l' aquifère alluvial de Wadi Halfayan est en principal alimenté par la recharge latérale provenant des ophiolites situées dans la partie est. Les plus importantes sources de recharge dans l'aval de l'aquifère de la Plaine Alluviale sont l'infiltration directe et le ruissellement provenant d'une source d'humidité qui s'approche d'Oman par le sud. Le modèle montre que la principale évolution géochimique se produise au long de la direction d'écoulement qui part de piémont de la Plaine Alluviale du Sud, où le procès de dédolomisation est responsable pour les changements observés dans la composition géochimique et en carbone des eaux.

Resumen Un modelo hidrogeoquímico regional fue desarrollado, para evaluar la evolución geoquímica de diferentes aguas subterráneas en un sistema acuífero aluvial ubicado en el interior de Omán. El modelo, en combinación con isótopos ambientales, es capaz de obtener información cualitativa y cuantitativa sobre recarga, direcciones de flujo de agua subterránea y sobre las conexiones hidráulicas entre diferentes acuíferos. La fuente principal de agua para el acuífero aluvial en el piedemonte son las aguas subterráneas, a lo largo de las direcciones de flujo del Wadi Abyadh y del Wadi M'uaydin, desde las áreas de gran altura de Jabal Akhdar y como infiltración local a lo largo de los canales del wadi. En contraste, el acuífero aluvial del piedemonte a lo largo del Wadi Halfayn, esta alimentado principalmente por recarga lateral desde las partes bajas de las

 DOI 10.1007/s10040-004-0425-2

montañas de ofiolitas hacia el Este, además por pequeñas contribuciones desde el Jabal Akhdar e infiltración local. Siguiendo gradiente abajo en el acuífero de la Llanura Aluvial del Sur, allí tanto la infiltración directa de lluvia, como la escorrentía superficial constituyen fuentes significativas de recarga, las cuales se originan en una fuente de humedad que llega a Omán proveniente del Sur. El modelo muestra, que la evolución geoquímica principal de las aguas subterráneas en el aluvión, sucede a lo largo de la dirección de flujo, que va desde el piedemonte hacia la Llanura Aluvial Sur, en donde el proceso de des-dolomitización es el responsable de los cambios observados en la composición química y también del contenido de isótopos de carbono en estas aguas.

## Introduction

This study focuses on the geochemical evolution of groundwaters in the Halfayn alluvial aquifer system in the interior (Dakhiliya region) of the Sultanate of Oman. The aquifer encompasses an area of approximately 4,000 km$^2$ and is the principal groundwater source for the whole region. Previous investigations in parts of the study area include Cansult/Gartner and Lee (1986) who described the origin and residence times of groundwater in the alluvial and bedrock aquifers in the Manah area between Manah and Adam based on environmental isotopes. Clark et al. (1987) presented a detailed isotope study on modern and fossil groundwater in Oman, including the data of Cansult/Gartner and Lee (1986) for the shallow alluvial and bedrock aquifers in the Halfayn system between Nizwa and Adam. A review of all available data of the entire Dakhiliya region from previous studies is presented in MWR (1995).

In arid regions, the assessment of available groundwater resources is key to the economic development and increased prosperity. In order to evaluate the existing groundwater resources and to develop improved water management strategies, it is primarily necessary to identify the dominant infiltration areas, sources of recharge and major groundwater flow paths as well as to estimate groundwater residence times. Many studies from semi-arid to arid areas have focused on the evaluation of recharge, its sources and spatial variability as well as the estimation of groundwater residence times by using mainly environmental isotopes and to a lesser extent hydrochemical data, e.g. chloride concentrations (e.g. Edmunds and Walton 1980; Adar and Neuman 1988; Issar et al. 1993; Edmunds and Gaye 1994; Simmers 1997; Weyhenmeyer et al. 2002; Macumber 2003).

This report presents results from a hydrogeochemical investigation that details the sources of recharge, the geochemical evolution along the flow paths, groundwater mixing of different water types and hydraulic connections between different aquifers from the high mountain areas through the piedmont region to the far alluvial plain. Radioisotopes are used to determine average groundwater residence times in the different aquifers and where applicable. Different recharge areas and moisture sources are proposed based on environmental isotope data and tested for their consistency with the overall geochemical evolution of the groundwaters. It is shown that a sound understanding of groundwater evolution including quantification by geochemical modeling refines the conclusions obtained from isotope studies alone.

## Hydrogeological setting

### *Study area*

The Halfayn alluvial aquifer system is located in Oman in the eastern part of the Dakhiliya Region, approximately 150 km southwest of the capital Muscat (Fig. 1). The area is characterized by a large alluvial plain, lining the flank of the Northern Oman Mountains (Fig. 1). To the north, the study area is bounded by the water divide of the Jabal Akhdar, a mountain chain rising up to 3,000 m. The southern limit is marked by the frontal ranges forming the Adam Mountains. The area has an arid climate with a mean annual precipitation of about 300 mm on the Jabal Akhdar and 90 mm on the alluvial plain (MWR 1995). Rainfall is characterized by large variability both in time and space. Precipitation is related to local summer convective storms and winter frontal storms, approaching from the north and northwest and originating from the Mediterranean Sea (Stanger 1986; Clark 1987; Macumber et al. 1997; Weyhenmeyer et al. 2002). Summer convective storms occur locally and are of short duration (min) compared to the frontal storms (h) during the winter months, whereby most of the rainfall occurs in the mountainous areas (Meteorological Reports, Ministry of Communications, Sultanate of Oman). Tropical cyclonic storms, originating in the southeastern Arabian Sea or the Bay of Bengal approach northern Oman occasionally and may cause heavy rainfall for several days. The frequency of these storms is estimated as once every 5–10 years (Taylor et al. 1990). In addition, low-pressure systems originating from the south (e.g. Horn of Africa) occasionally approach northern Oman and are the source for sporadic but heavy rainfall in this area (Macumber 2003). The mean annual temperature is between 17°C in the high mountain areas and 28°C in the low-lying alluvial plain (MWR 1995). Natural vegetation and soil development is almost absent in the mountainous areas, where bedrock is exposed, and sparse in the alluvial plain.

### *Geology and hydrostratigraphy*

The alluvial plain of the Halfayn System lies in a synclinal basin between the Jabal Akhdar to the north and the Adam Mountains to the south (Fig. 2). The geology of northern Oman has been described in detail by Glennie et al. (1974) and Robertson et al. (1990). Gibb and Partner (1976) first discussed the hydrogeology of the area. A simplified hydrostratigraphic map and a schematic cross-section are illustrated in Figs. 1 and 2. Table 1 summarizes the major hydrostratigraphic units of the study area.

 DOI 10.1007/s10040-004-0425-2

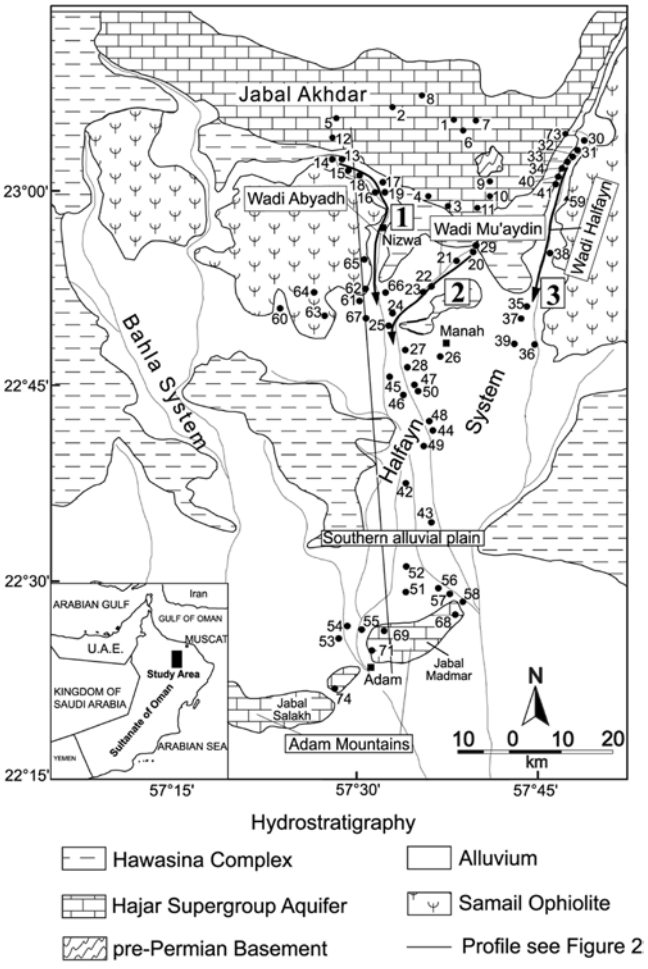


**Fig. 1** Location of the study area (*inset map*) and simplified hydrostratigraphic map with locations of boreholes (*solid circles*). The *arrows* indicate the flow paths in the alluvial piedmont area

The pre-Permian basement or the Autochthonous Unit A of Glennie et al. (1974) consists mainly of thinly laminated siltstones and phyllites that form the core of the Jabal Akhdar anticline. Stanger (1986) interpreted these pre-Permian sediments as an aquitard based on non-productive boreholes, the absence of springs in the unit and the occurrence of numerous springs along the unconformable contact with the overlying Permian to Cretaceous carbonates.

**Table 1** Hydrostratigraphic and lithostratigraphic summary for the Halfayn alluvial aquifer system

| Hydrostratigraphy | Rock type | Aquifer type |
|---|---|---|
| Alluvium | gravel, sand, silt, clay | alluvial aquifer |
| Samail Ophiolite (Allochthonous) | tectonized harzburgite gabbro | fractured aquifer |
| Hawasina Complex (Allochthonous) | limestones, radiolarites, shales | aquitard |
| Aruma Group | siltstones, shales | aquiclude |
| Hajar Supergroup | limestones, dolomites | fractured and karstified aquifer |
| Pre-Permian Basement | siltstones (phyllites) | aquitard |

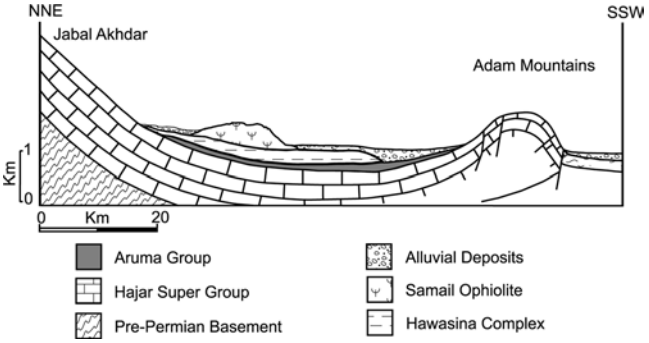


**Fig. 2** Schematic cross-section through the synclinal basin from the Jabal Akhdar in the NNE to the frontal Adam Mountains in the SSW (see Fig. 1 for location)

The Permian to Cretaceous Hajar Supergroup carbonates, representing the Autochthonous Unit B of Glennie et al. (1974), form essentially the large anticline of the Jabal Akhdar. On its southern flank, the carbonate rocks dip steeply beneath the alluvial plain and re-emerge 80 km further south in the frontal Adam Mountains (Fig. 2). They build the main regional bedrock aquifer, and are described by Stanger (1986) as the "Hajar Supergroup aquifer." The carbonaceous sequence consists mainly of shallow marine bioclastic and clayey limestones and dolomites—with a total thickness between 2,000 and 3,000 m (Rabu et al. 1990). The aquifer is heterogeneous and anisotropic due to an extensive fracture network and karstic features. The transmissivities of fractured limestones and dolomites range from $2\times10^{-5}$ to maximum $1.8\times10^{-2}$ m$^2$/s and storage coefficients vary from 0.0015 to 0.34 according to pump tests (MacDonald 1982, 1994; MWR 1996).

The Permian to Cretaceous carbonates are unconformably overlain by Late Cretaceous siltstones and shales of the Aruma Group (Glennie et al. 1974), where it forms a confining layer. The total thickness varies between 80 and 150 m on the southern edge of the Jabal Akhdar (Rathmayr 2000).

Half of the study area is covered or is underlain at shallow depth by Permian to Cretaceous turbiditic limestones, radiolarites and siltstones of the allochthonous Hawasina Nappes (Glennie et al. 1974). These sediments are intensely folded and faulted due to nappe displacement (Robertson et al. 1990). No springs are known to originate from these deep marine sediments and boreholes drilled into this unit are in general non-productive (Stanger 1986; MWR 1995).

The ophiolitic rocks of the Samail Ophiolite, a fragment of obducted mid-Cretaceous oceanic lithosphere (Lippard et al. 1986; Peters et al. 1990) are exposed in a number of structural blocks, which form the foothills of the Jabal Akhdar to the south and southeast (Fig. 1). Variably tectonized peridotites, mainly harzburgite, cut by numerous pyroxenite dykes are the major ophiolitic rock types. The primary composition of the peridotite is olivine, orthopyroxene (enstatite) and minor clinopy-


DOI 10.1007/s10040-004-0425-2

roxene (diopside) (Pallister and Hopson 1981). Strong serpentinization however changed the primary mineralogy and secondary minerals such as serpentine, brucite and magnesite are more abundant (Neal and Stanger 1985). Serpentinization reduced the overall hydraulic conductivity of the peridotites. However, fracturing during the tectonic emplacement led to intense weathering down to some tens of meters of depth that resulted in a considerable increase in the near-surface porosity. The peridotites form locally restricted aquifers and few boreholes drilled recently into the weathered and fractured peridotites gave yields of maximum 50 l/s (MWR 1994). Pump tests revealed transmissivities in the range of $8\times10^{-5}$ to $1\times10^{-4}$ $m^2/s$ and an average storage coefficient of $8\times10^{-4}$ for fractured and weathered peridotites (MWR 1994).

Up to maximum 80 m thick Quaternary alluvial deposits are accumulated in N–S trending wadi systems in the Jabal Akhdar and in large alluvial fans, forming the Southern Alluvial Plain. Besides many small tributary wadi channels, Wadi Abyadh, Wadi Mu'aydin and Wadi Halfayn are the main active wadi systems, which all originate in the Jabal Akhdar mountains (Fig. 1). Surface water flow in these wadi channels is ephemeral and only occurs after heavy rainfall events. During such events, significant groundwater recharge occurs along the active wadi channels (e.g. Matter 2001). The alluvial deposits are composed of coarse to fine-grained gravels of varying lithological composition, sand, silt and clay (Stanger 1986). Evaporitic salt and gypsum crusts, formed after short duration rainfalls, occur at the surface and in near-surface layers in small depressions (Stalder 1975). Fibrous gypsum and traces of halite in association with fine gravels are widespread in the alluvial sequence of the Halfayn system (Atkins 1986). The cementation of the alluvial deposits is very heterogeneous in time as well as in space and comprises high-magnesium calcite, low-magnesium calcite and dolomite (Stanger 1986; Burns and Matter 1995). Poorly to weakly cemented gravels, which form the lowermost alluvial deposits, are partially embedded in a sandy to silty matrix or granular gypsum matrix (Stanger 1986). They either overlie weathered or fresh bedrock. The alluvial aquifer in the wadi Halfayn system is partly unconfined in the northern piedmont area and changes to semi-confined and confined conditions in the Southern Alluvial Plain, where silt deposits of up to 10 m thickness act as a local confining layer. Reported transmissivities for the weakly to uncemented gravels with sand and silt layers, which form the principal alluvial aquifer, range from $5\times10^{-4}$ to $10^{-2}$ $m^2/s$ on the basis of aquifer pump tests (MWR 1995). The average hydraulic gradient is about 5 m/km in the piedmont zone and about 1 m/km in the Southern Alluvial Plain with a general groundwater flow from north to south.

## Methods

### Water sampling, chemical and isotopic analyses

Over 70 boreholes, evenly distributed over the study area were sampled during three field campaigns between 1997 and 1999. In addition, several ephemeral and perennial springs were sampled in the Jabal Akhdar and the foothills. The locations of the boreholes and the springs are illustrated in Fig. 1. Water sampling by pumping occurred after pH, temperature, dissolved oxygen concentration and electrical conductivity of the effluent had reached stable values (e.g. pH $\pm$ 0.1). All boreholes are equipped with discrete screen intervals except for those in the limestones and dolomites of Hajar Supergroup aquifer. All groundwater samples were collected in polyethylene or glass bottles for analysis of major ion chemistry and stable isotopes ($\delta^2H$, $\delta^{18}O$, $\delta^{13}C$), respectively.

Major and minor ions, alkalinity and selected trace elements were analyzed at the Chemistry Laboratory of the Ministry of Water Resources in Muscat within 2 weeks of sampling. Cations were analyzed by standard ICP (inductively coupled plasma spectrometry), anions by ion chromatography and trace elements were analyzed by atomic adsorption spectroscopy. The chemical analyses were only accepted when the ion charge balance was better than $\pm5\%$.

Stable isotope ratios of oxygen and hydrogen were analyzed with a VG-Prism II isotope ratio mass spectrometer (IRMS) at the Institute of Geological Sciences, University of Bern, Switzerland. Oxygen isotope ratios were measured by $CO_2$ equilibration of the water sample, while hydrogen isotopes were measured by in-line equilibration with platinum-coated "Hokko beads" (see Matter 2001 and Weyhenmeyer et al. 2002 for details). The results are expressed in $\delta$‰with respect to Vienna Standard Mean Ocean Water (VSMOW; Gonfiantini 1978) and the overall analytical accuracy was $\pm0.1$‰for $\delta^{18}O$, $\pm0.6$‰for $\delta^2H$. For carbon and oxygen isotope measurements of dissolved inorganic carbon from water or rock samples, water or powdered rock material was reacted under vacuum with anhydrous (100%) $H_3PO_4$ and the liberated $CO_2$ was directly released into the VG-Prism II mass spectrometer. The overall analytical accuracy for $\delta^{13}C$ and $\delta^{18}O$ is $\pm0.1$‰and all the analyses are reported relative to the PDB standard. All the samples were corrected using the phosphoric acid fractionation factor for calcite at the appropriate temperature (Swart et al. 1991). Tritium activities in groundwater samples and measurements of radiocarbon ($^{14}C$) on precipitated $BaCO_3$ were carried out using liquid scintillation counting technique by Hydroisotop GmbH, Schweitenkirchen, Germany. For the $^{14}C$-measurements dissolved carbon was precipitated as $BaCO_3$ in the field by adding NaOH and $BaCl_2$ to 80 l of groundwater. The reported precision ($2\sigma$) of the tritium analyses was $\pm0.5$ TU and the absolute error range for $^{14}C$ measurements was between $\pm1.0$ and $\pm3.1$ pmC (percent modern carbon).

### Geochemical modeling

The distribution of aqueous species in the groundwaters and mineral saturation states (SI = log IAP/$K_T$, where IAP is the ion activity product and $K_T$ is the equilibrium constant at temperature $T$) were calculated using the geochemical code PHREEQC (v. 2, Parkhurst and Appelo 1999) and

 DOI 10.1007/s10040-004-0425-2

the WATEQ4F (Ball and Nordstrom 1991) thermodynamic database. The same code was applied for inverse modeling (mass balance) including mixing of different waters to evaluate the proportions of various potential sources to the groundwater in the piedmont area of Wadi Halfayn. In such calculations an uncertainty in the chemical concentrations of maximum 5% was allowed to account for the overall analytical error. The absolute error for the $\delta^{18}O$ value of the groundwaters was set to ±0.1‰, that for the $\delta^{13}C$ of reacting calcite to ±1.0‰, and that for $\delta^{13}C$ of reacting dolomite, high-magnesium calcite and $CO_{2(gas)}$ to ±2.0‰due to the larger observed spread in these latter data. Models were accepted if the mixing fractions calculated for the conservative tracers Cl and $\delta^{18}O$ agree with each other and if the resulting composition and mineral mass transfer of the mixture is consistent with the observed composition and mineral saturation state of the target groundwater.

The evolution of the alluvial groundwater from the piedmont area to the Southern Alluvial Plain was evaluated with reaction path calculations using PHREEQC. In these calculations dissolved Cl is used as a reaction progress variable along the flow path and the simulated groundwater compositions and mineral saturation states are compared to those measured along the flow path.

Where applicable, $^{14}C$-residence times were calculated with the geochemical code NETPATH (v. 2.0, Plummer et al. 1994). In these calculations the total inorganic carbon (TIC) inventory of the groundwater was corrected for exchange with soil-$CO_2$ and dilution with $^{14}C$-free carbon from carbonate mineral reactions. Modeled $^{14}C$-residence times were only considered geologically meaningful if the calculated mineral mass transfer (i.e. dissolution vs. precipitation) and the $\delta^{13}C_{TIC}$ were in agreement with the calculated mineral saturation state of the groundwater and the measured $\delta^{13}C_{TIC}$, respectively.

## Results

### Groundwater chemistry

#### *Hajar Supergroup aquifer*

Boreholes penetrating the limestones and dolomites of the Hajar Supergroup aquifer are restricted to the Jabal Akhdar in the north and the Adam Mountains in the south (Fig. 1). Due to the fractured and karstic flow system it was neither possible to collect groundwater samples along a continuous flow path within the Hajar Supergroup aquifer of the Jabal Akhdar nor of the Adam Mountains. Groundwater in the recharge areas of the Jabal Akhdar is of a Ca–Mg–$HCO_3$ type water with a total dissolved solid content (TDS) between 315 and 550 mg/l. Groundwater in the Adam Mountains is much higher mineralized (TDS: 1,477—3,093 mg/l) and of a Na–Mg–Cl–$SO_4$–$HCO_3$ or Na–Cl type water (Table 2; Fig. 3). Some of these groundwaters are further characterized by a persistent smell of $H_2S$ indicating reducing conditions in the underground.

The Ca–Mg–$HCO_3$ type groundwaters of the Hajar Supergroup aquifer of the Jabal Akhdar are typical for limestone and dolomite dominated environments, while those of the Adam Mountains indicate a more complex evolution.

#### *Ophiolite aquifer*

Surface and shallow groundwater within the tectonized peridotites are of a Mg–(Na)–$HCO_3$–(Cl) type (Fig. 3) with pH-values between 7.0 and 8.5 and TDS contents between 245 and 1,187 mg/l (Table 2). The predominant hydrochemical characteristic of surface as well as shallow groundwater from the ophiolite aquifer is the high Mg/Ca ratio. The molar ratios range between 2.94 and 6.25 (Table 2). Average magnesium concentrations measured in groundwater samples are 2.70 mmol/l ($n$=8), compared to average calcium concentrations of 0.67 mmol/l. The shallow groundwaters therefore differ from deep ophiolite groundwaters as described e.g. by Neal and Stanger (1985) and Stanger (1986).

#### *Alluvial aquifer*

In the alluvial aquifer, groundwater evolves from low mineralized Ca–Mg–$HCO_3$ or Mg–Ca–$HCO_3$ type water (TDS: <600 mg/l) in the piedmont area to more mineralized Na–Mg–(Ca)–Cl–$SO_4$–$HCO_3$ type water (TDS: maximum 1,940 mg/l) in the Southern Alluvial Plain, north of the Adam Mountains (Fig. 4). Based on borehole location, piezometric surface and chemical composition of the groundwater, three flow paths that correspond to different sub-catchments can be distinguished in the alluvial piedmont area of the Halfayn system (Fig. 1). Along flow path 1 and 2, following Wadi Abyadh and Mu'aydin, respectively,

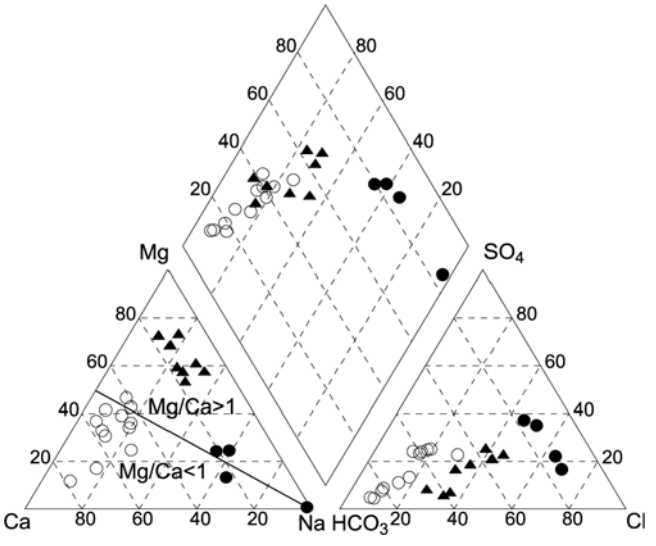


**Fig. 3** Piper Diagram illustrating the chemical composition of groundwater from the Hajar Supergroup aquifer of the Jabal Akhdar (*open dots*) and the Adam Mountains (*solid dots*), and from the ophiolite aquifer (*solid triangles*). The detailed chemical analyses for each sample are listed in Table 2


DOI 10.1007/s10040-004-0425-2

**Table 2** Selected chemical properties of groundwater samples from the different aquifers

| No | Well ID | TDS (mg/l) | *T* (°C) | pH[a] | Ca (mmol/l) | Mg (mmol/l) | Na (mmol/l) | K (mmol/l) | Si (mmol/l) | $HCO_3^-$ (mmol/l) | Cl (mmol/l) | $SO_4$ (mmol/l) | $NO_3$ (mmol/l) | Mg/Ca |
|---|---|---|---|---|---|---|---|---|---|---|---|---|---|---|
| Hajar Supergroup Aquifer: Jabal Akhdar | | | | | | | | | | | | | | |
| 1 | JA05 | 498 | 22.0 | 7.08 | 1.92 | 1.56 | 0.57 | 0.03 | 0.18 | 6.00 | 0.68 | 0.16 | 0.03 | 0.81 |
| 2 | JA17 | 550 | 23.8 | 7.20 | 1.77 | 1.48 | 1.08 | 0.04 | 0.22 | 4.67 | 1.01 | 0.90 | 0.06 | 0.84 |
| 3 | SP03 | 413 | 23.0 | 7.25 | 2.22 | 0.33 | 0.56 | 0.03 | 0.22 | 5.03 | 0.56 | 0.23 | 0.04 | 0.15 |
| 4 | SP04 | 421 | 28.1 | 7.30 | 1.92 | 0.49 | 0.95 | 0.03 | na | 3.06 | 0.97 | 0.36 | 0.06 | 0.26 |
| 5 | SP05 | 441 | 30.3 | 7.24 | 1.67 | 0.90 | 0.82 | 0.03 | 0.19 | 1.75 | 1.10 | 0.59 | 0.05 | 0.54 |
| 6 | SP06 | 427 | 23.0 | 7.43 | 0.95 | 1.07 | 0.56 | 0.02 | na | 5.25 | 0.65 | 0.23 | 0.07 | 1.13 |
| 7 | SP07 | 397 | 22.3 | 7.33 | 1.54 | 0.90 | 0.61 | 0.02 | 0.14 | 1.53 | 0.76 | 0.23 | 0.17 | 0.58 |
| 8 | SP08 | 496 | 23.7 | 7.08 | 1.89 | 1.23 | 0.43 | 0.02 | 0.17 | 6.57 | 0.53 | 0.15 | 0.03 | 0.65 |
| 9 | SP09 | 325 | 28.5 | 7.62 | 0.85 | 0.87 | 0.69 | 0.04 | na | 1.60 | 0.76 | 0.46 | 0.03 | 1.02 |
| 10 | SP10 | 315 | 22.3 | 7.72 | 0.86 | 0.69 | 0.78 | 0.06 | na | 1.53 | 0.71 | 0.43 | 0.11 | 0.80 |
| 11 | NSA32 | 316 | 32.5 | 7.36 | 1.34 | 0.98 | 1.13 | 0.04 | 0.21 | 3.17 | 1.10 | 0.71 | 0.02 | 0.73 |
| 12 | NSA09 | 663 | 33.0 | 7.00 | 2.34 | 1.39 | 4.29 | 0.11 | 0.23 | 4.80 | 4.71 | 1.16 | 0.08 | 0.59 |
| 73 | JA10S | 271 | 32.7 | 7.33 | 1.10 | 0.99 | 0.74 | 0.04 | 0.22 | 4.35 | 0.76 | 0.30 | 0.04 | 0.90 |
| Hajar Supergroup Aquifer: Adam Mountains | | | | | | | | | | | | | | |
| 68 | AA01 | 1,747 | 38.4 | 7.11 | 2.48 | 3.37 | 16.12 | 0.28 | 0.48 | 4.40 | 14.55 | 5.49 | 0.04 | 1.36 |
| 69 | ADM03 | 1,525 | 41.0 | 7.06 | 2.56 | 2.92 | 13.50 | 0.20 | 0.43 | 4.09 | 10.39 | 4.26 | 0.04 | 1.14 |
| 71 | ADM01 | 3,093 | 37.8 | 7.68 | 0.45 | 0.33 | 43.55 | 0.33 | 0.29 | 7.22 | 34.09 | 4.29 | 0.03 | 0.73 |
| 74 | AA07 | 1,729 | 38.9 | 7.12 | 2.65 | 2.47 | 17.99 | 0.23 | 0.45 | 4.31 | 16.16 | 4.60 | 0.07 | 0.93 |
| Ophiolite Aquifer | | | | | | | | | | | | | | |
| 59 | WHF09R | 328 | 34.5 | 7.87 | 0.38 | 1.57 | 0.48 | 0.03 | 0.38 | 2.99 | 1.64 | 0.10 | 0.10 | 4.13 |
| 60 | SHD11R | 456 | 35.3 | 7.67 | 0.60 | 2.02 | 1.87 | 0.07 | 0.53 | 3.42 | 2.03 | 0.52 | 0.18 | 3.37 |
| 61 | F2204 | 245 | 30.2 | 8.53 | 0.25 | 1.44 | 1.39 | 0.64 | na | 1.19 | 1.44 | 0.34 | 0.09 | 5.76 |
| 62 | F2221 | 781 | 29.7 | 7.66 | 0.52 | 3.25 | 3.87 | 0.13 | na | 5.51 | 4.26 | 1.06 | 0.11 | 6.25 |
| 63 | F0474 | 397 | 33.7 | 7.74 | 0.47 | 2.06 | 1.00 | 0.06 | na | 3.69 | 1.44 | 0.21 | 0.20 | 4.38 |
| 64 | F0473 | 438 | 30.5 | 7.93 | 0.35 | 2.43 | 1.13 | 0.06 | na | 3.63 | 2.17 | 0.19 | 0.32 | 6.94 |
| 66 | WNZ21A | 810 | 34.5 | 7.00 | 1.12 | 3.29 | 3.66 | 0.13 | 0.52 | 4.71 | 5.70 | 1.39 | 0.21 | 2.94 |
| 67 | WNZ08 | 1,187 | 35.5 | 7.07 | 1.67 | 5.52 | 4.40 | 0.23 | 0.66 | 7.44 | 6.81 | 2.20 | 0.38 | 3.31 |
| Alluvial Aquifer: Piedmont | | | | | | | | | | | | | | |
| Flow path 1 | | | | | | | | | | | | | | |
| 13 | NSA15 | 364 | 33.2 | 7.35 | 1.54 | 0.81 | 0.61 | 0.04 | 0.21 | 2.54 | 1.69 | 0.28 | 0.20 | 0.53 |
| 14 | F5 | 512 | 33.4 | 7.12 | 2.09 | 1.31 | 1.04 | 0.05 | 0.28 | 4.08 | 2.37 | 0.46 | 0.34 | 0.63 |
| 15 | F6 | 427 | 29.8 | 7.24 | 1.67 | 0.94 | 0.95 | 0.05 | 0.21 | 3.98 | 1.16 | 0.44 | 0.15 | 0.56 |
| 16 | NTF6 | 406 | 34.7 | 7.28 | 1.36 | 1.07 | 0.87 | 0.05 | 0.40 | 3.32 | 1.24 | 0.30 | 0.22 | 0.79 |
| 17 | WNZ4R | 574 | 33.5 | 6.95 | 2.34 | 1.35 | 1.13 | 0.04 | 0.42 | 5.84 | 1.58 | 0.55 | 0.17 | 0.58 |
| 18 | NSA16B | 437 | 33.3 | 7.21 | 1.45 | 0.96 | 0.91 | 0.05 | 0.31 | 3.08 | 1.38 | 0.27 | 0.21 | 0.66 |
| 19 | JM247F | 373 | 32.3 | 7.34 | 1.34 | 0.98 | 0.74 | 0.05 | 0.33 | 3.45 | 1.18 | 0.29 | 0.17 | 0.73 |
| Flow path 2 | | | | | | | | | | | | | | |
| 20 | NSA17 | 320 | 32.2 | 7.50 | 1.07 | 0.61 | 0.87 | 0.05 | 0.27 | 2.55 | 0.62 | 0.42 | 0.13 | 0.57 |
| 21 | APM1 | 311 | 33.0 | 7.64 | 0.74 | 0.72 | 1.04 | 0.05 | na | 2.60 | 0.79 | 0.41 | 0.04 | 0.97 |
| 22 | APM6 | 423 | 33.8 | 7.28 | 1.32 | 0.98 | 0.91 | 0.06 | na | 3.80 | 0.82 | 0.38 | 0.14 | 0.74 |
| 23 | APM7 | 441 | 33.9 | 7.22 | 1.36 | 0.83 | 0.78 | 0.05 | 0.27 | 3.83 | 0.68 | 0.39 | 0.14 | 0.61 |
| 24 | APM10 | 309 | 34.6 | 7.55 | 0.82 | 1.11 | 2.04 | 0.04 | 0.53 | 3.25 | 1.21 | 0.50 | 0.19 | 1.35 |
| 25 | APM15 | 425 | 32.9 | 7.21 | 1.28 | 1.26 | 2.43 | 0.05 | 0.50 | 4.60 | 1.58 | 0.53 | 0.17 | 0.98 |
| 26 | MN21 | 276 | 35.2 | 7.35 | 1.18 | 0.83 | 0.95 | 0.05 | 0.43 | 3.09 | 0.73 | 0.37 | 0.16 | 0.70 |
| 27 | MN24 | 381 | 33.8 | 7.10 | 1.47 | 1.12 | 1.69 | 0.06 | 0.41 | 3.93 | 1.35 | 0.52 | 0.16 | 0.76 |
| 28 | MN9-01 | 423 | 36.0 | 6.90 | 1.16 | 1.52 | 2.34 | 0.07 | 0.59 | 4.37 | 1.67 | 0.55 | 0.13 | 1.31 |
| 29 | JM243F | 413 | 30.5 | 7.29 | 1.47 | 0.98 | 0.82 | 0.05 | na | 3.94 | 0.95 | 0.53 | 0.29 | 0.67 |
| 45 | MN16-01 | 490 | 35.5 | 7.00 | 0.62 | 1.52 | 2.87 | 0.10 | 0.48 | 3.39 | 2.14 | 0.67 | 0.17 | 2.45 |
| Flow path 3 | | | | | | | | | | | | | | |
| 30 | APH15 | 463 | 32.8 | 7.23 | 1.17 | 1.63 | 0.78 | 0.05 | na | 4.06 | 1.07 | 0.24 | 0.15 | 1.39 |
| 31 | APH1 | 375 | 32.9 | 7.46 | 0.80 | 1.40 | 0.74 | 0.05 | na | 3.80 | 0.71 | 0.20 | 0.18 | 1.75 |
| 32 | APH5 | 276 | 29.8 | 7.63 | 0.71 | 0.83 | 0.35 | 0.05 | 0.34 | 2.99 | 0.28 | 0.14 | 0.14 | 1.17 |

 DOI 10.1007/s10040-004-0425-2

**Table 2** Continued

| | | | | | | | | | | | | | | |
|---|---|---|---|---|---|---|---|---|---|---|---|---|---|---|
| 33 | APH4 | 422 | 31.4 | 7.43 | 0.95 | 1.35 | 0.48 | 0.04 | na | 3.97 | 0.65 | 0.18 | 0.15 | 1.42 |
| 34 | APH3 | 442 | 32.2 | 7.28 | 1.02 | 1.76 | 0.52 | 0.05 | na | 4.80 | 0.82 | 0.1 | 0.14 | 1.73 |
| 35 | APH8 | 695 | 33.8 | 7.40 | 0.86 | 2.67 | 3.21 | 0.11 | na | 4.60 | 3.73 | 0.86 | 0.17 | 3.10 |
| 36 | WHF3R | 691 | 33.1 | 7.41 | 0.98 | 2.27 | 3.69 | 0.12 | 0.43 | 3.99 | 4.71 | 0.88 | 0.20 | 2.32 |
| 37 | APH07 | 522 | 32.8 | 7.56 | 0.58 | 1.22 | 3.08 | 0.08 | na | 4.39 | 2.37 | 0.39 | 0.10 | 2.10 |
| 38 | NSA18B | 856 | 32.3 | 7.24 | 0.99 | 3.25 | 3.55 | 0.11 | 0.55 | 6.39 | 3.61 | 1.07 | 0.25 | 3.28 |
| 39 | WHF4R | 741 | 34.9 | 7.38 | 0.98 | 2.92 | 3.34 | 0.10 | na | 4.19 | 4.91 | 0.98 | 0.18 | 2.98 |
| 40 | APH02 | 362 | 32.4 | 7.36 | 0.95 | 1.48 | 0.48 | 0.04 | 0.43 | 4.63 | 0.31 | 0.14 | 0.16 | 1.56 |
| 41 | APH12 | 427 | 32.3 | 7.28 | 1.17 | 1.40 | 0.78 | 0.04 | 0.37 | 4.74 | 0.82 | 0.23 | 0.16 | 1.20 |
| Alluvial Aquifer: Southern Alluvial Plain | | | | | | | | | | | | | | |
| 42 | MN5-01 | 1,024 | 35.9 | 7.30 | 1.25 | 2.35 | 6.91 | 0.18 | 0.60 | 3.57 | 6.95 | 1.92 | 0.18 | 1.87 |
| 43 | MN3-03 | 1,001 | 35.7 | 7.32 | 1.32 | 2.86 | 7.73 | 0.18 | 0.61 | 4.35 | 6.92 | 2.23 | 0.09 | 2.17 |
| 44 | MN8-01 | 1,161 | 36.1 | 7.10 | 1.50 | 3.05 | 8.14 | 0.21 | 0.62 | 4.79 | 7.82 | 2.66 | 0.08 | 2.03 |
| 46 | NWS4 | 531 | 36.1 | 7.50 | 0.75 | 1.85 | 2.70 | 0.09 | 0.57 | 4.00 | 1.92 | 0.72 | 0.14 | 2.47 |
| 47 | NWS10 | 748 | 34.6 | 7.34 | 1.05 | 2.31 | 4.61 | 0.11 | 0.65 | 4.81 | 3.27 | 1.27 | 0.12 | 2.20 |
| 48 | NWS15 | 1,282 | 34.7 | 7.27 | 1.50 | 3.75 | 9.67 | 0.23 | 0.71 | 4.81 | 8.67 | 3.04 | 0.09 | 2.50 |
| 49 | NWS6 | 941 | 34.7 | 7.38 | 1.12 | 2.63 | 6.79 | 0.17 | 0.58 | 4.40 | 5.84 | 1.93 | 0.13 | 2.35 |
| 50 | NWS5 | 851 | 34.0 | 7.34 | 1.10 | 2.51 | 5.88 | 0.13 | 0.59 | 4.81 | 4.46 | 1.53 | 0.11 | 2.28 |
| 51 | NSA33A | 1,366 | 35.5 | 7.21 | 1.82 | 4.08 | 9.50 | 0.22 | 0.70 | 4.61 | 9.29 | 3.63 | 0.09 | 2.24 |
| 52 | NSA35A | 1,022 | 35.5 | 7.28 | 1.33 | 2.93 | 7.14 | 0.18 | 0.63 | 4.50 | 6.30 | 2.25 | 0.10 | 2.20 |
| 53 | AG04 | 1,313 | 35.1 | 7.40 | 1.50 | 2.55 | 12.33 | 0.28 | 0.51 | 3.30 | 13.33 | 2.24 | 0.11 | 1.70 |
| 54 | AG33 | 1,381 | 36.0 | 7.37 | 1.55 | 2.93 | 11.80 | 0.27 | 0.49 | 3.54 | 13.35 | 2.85 | 0.02 | 1.89 |
| 55 | AG35 | 986 | 36.3 | 7.29 | 1.37 | 3.04 | 7.45 | 0.19 | 0.63 | 4.40 | 7.45 | 2.46 | 0.11 | 2.22 |
| 56 | WH10 | 1,698 | 35.1 | 7.19 | 2.00 | 3.21 | 13.03 | 0.27 | 0.64 | 4.71 | 12.70 | 4.31 | 0.03 | 1.61 |
| 57 | WH27 | 1,651 | 35.0 | 7.17 | 1.95 | 3.75 | 14.03 | 0.30 | 0.63 | 5.54 | 12.18 | 4.16 | 0.17 | 1.92 |
| 58 | WH21 | 1,940 | 35.3 | 7.13 | 2.10 | 4.20 | 17.08 | 0.32 | 0.69 | 6.03 | 14.61 | 5.13 | 0.13 | 2.00 |

Well ID refers to the registered borehole name of the Ministry of Water Resources, Sultanate of Oman

[a]Adjusted for calcite saturation

the groundwater is of a Ca–Mg–$HCO_3$ type (Fig. 4) with Mg/Ca ratios generally below one (Table 2). The groundwater originates from the Jabal Akhdar mountains, which are dominated by the calcareous lithologies of the Hajar Supergroup. Groundwater along flow path 3, following the Wadi Halfayn, is of a Mg–Ca–$HCO_3$ type. The predominant hydrochemical characteristic along flow path 3 is the continuous increase in the molar Mg/Ca ratio from 1.17 to 3.28 (Table 2). South of the piedmont area, the groundwaters of the three flow paths gradually merge and a strong increase in the magnesium, calcium, sulfate, sodium and chloride concentrations is observed from north to south in the Southern Alluvial Plain (Figs. 5 and 6).

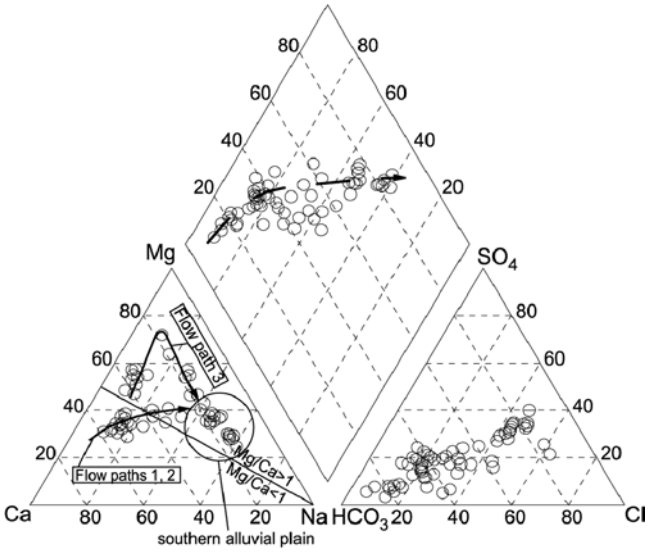


**Fig. 4** Piper diagram showing the chemical evolution of the alluvial groundwater along different flow paths in the piedmont area and in the confluence zone of the southern alluvial plain. The detailed chemical data is listed in Table 2 and the flow paths are indicated in Fig. 1

## *Stable isotopes*

### *Oxygen and hydrogen isotope composition ($\delta^{18}O\delta^{2}H$)*

The water isotope composition of groundwater sampled from the different aquifers of the Halfayn system shows distinct differences (Table 3). Groundwater from the Hajar Supergroup aquifer is depleted in $^{18}O$ and $^{2}H$ (Jabal Akhdar: $\delta^{18}O_{mean} = -2.9‰$, $\delta^{2}H_{mean} = -11.1‰$; Adam Mountains: $\delta^{18}O_{mean} = -2.8‰$, $\delta^{2}H_{mean} = -16.1‰$) compared to that from the ophiolite aquifer ( $\delta^{18}O_{mean} = -0.9‰$, $\delta^{2}H_{mean} = -1.9‰$) and alluvial aquifer ( $\delta^{18}O_{mean} = -1.9‰$, $\delta^{2}H_{mean} = -8.4‰$) aquifer. As shown below, these differences can be related to differences in recharge altitude and dominant moisture source (i.e. precipitation from northern and southern directions, respectively).

 DOI 10.1007/s10040-004-0425-2

**Table 3** Sample site locations, well data and selected isotope values of groundwater samples from wells, springs and aflaj located in the different aquifers

| No | Well name | Altitude (m a.s.l.) | Well depth (m.b.s.) | Depth screen (m.b.s.) | $\delta^{18}O$ (‰) | $\delta^{2}H$ (‰) | $\delta^{13}C$ (‰) | $^{14}C$ (pmc) | $^{3}H$ (TU) |
|---|---|---|---|---|---|---|---|---|---|
| Hajar Supergroup Aquifer: Jabal Akhdar | | | | | | | | | |
| 1 | JA05 | 1,950 | na | Open | −3.7 | −19.1 | −8.50 | 54.1±3.1 | 2.1±1.0 |
| 2 | JA17 | 1896.4 | 339 | Open | −3.5 | −13.2 | −6.19 | 46.6±1.0 | 4.2±1.0 |
| 3 | SP03 | 620 | – | Spring | −2.5 | −4.9 | na | na | na |
| 4 | SP04 | 730 | – | Spring | −2.0 | −6.5 | na | na | na |
| 5 | SP05 | 800 | – | Spring | −3.3 | −12.8 | na | na | na |
| 6 | SP06 | 1,900 | – | Spring | −3.4 | −15.3 | na | na | 3.8 |
| 7 | SP07 | 1,950 | – | Spring | −2.9 | −13.6 | na | na | na |
| 8 | SP08 | 2,000 | – | Spring | −3.6 | −16.2 | na | na | na |
| 9 | SP09 | 1,200 | – | Spring | −2.7 | −4.6 | na | na | na |
| 10 | SP10 | 850 | – | Spring | −1.6 | −2.5 | na | na | na |
| 11 | NSA32 | 705 | 400 | Open | −2.6 | −10.4 | −7.10 | 35.4±1.7 | 0.5±0.5 |
| 12 | NSA09 | 616.2 | 268.7 | Open | −2.9 | −15.6 | −7.30 | 44.1±2.9 | na |
| 73 | JA10S | 696.3 | 58 | 36.0 | −3.1 | −9.1 | na | na | 1.5±1.0 |
| Hajar Supergroup Aquifer: Adam Mountains | | | | | | | | | |
| 68 | AA01 | 312.8 | 91 | 48.3 | −2.4 | −13.3 | −9.80 | 40.9±1.6 | <0.5 |
| 69 | ADM03 | 327.8 | 151 | 122.0 | −2.4 | −12.2 | −10.58 | 30.9±2.4 | <0.4 |
| 71 | ADM01 | 302.8 | 329 | Open | −3.9 | −29.5 | −6.70 | 0.0±0.3 | <0.1 |
| 74 | AA07 | 306.8 | 100.5 | 76.5 | −2.6 | −12.6 | na | na | <0.5 |
| Ophiolite Aquifer | | | | | | | | | |
| 59 | WHF09R | 595.8 | 47 | 29.5 | −1.4 | −4.5 | −15.56 | na | 7.8±1.8 |
| 60 | SHD11R | 531.3 | 30 | 21.0 | −1.0 | −6.1 | −13.60 | na | na |
| 61 | F2204 | 450 | – | Falaj | −0.6 | −0.5 | na | na | na |
| 62 | F2221 | 455 | – | Falaj | −0.9 | 0.5 | na | na | na |
| 63 | F0474 | 460 | – | Falaj | −0.6 | 5.4 | na | na | na |
| 64 | F0473 | 470 | – | Falaj | −0.6 | 2.9 | na | na | na |
| 66 | WNZ21A | 460.6 | 36 | 26.0 | −1.2 | −2.7 | na | na | na |
| 67 | WNZ08 | 439.2 | 32 | 14.0 | −0.8 | −9.9 | na | na | na |
| Alluvial Aquifer: Piedmont | | | | | | | | | |
| Flow path 1 | | | | | | | | | |
| 13 | NSA15 | 601.7 | 49.4 | 38.2 | −2.6 | −10.0 | na | na | na |
| 14 | F5 | 602.5 | 44 | na | −2.1 | −9.2 | na | na | 4.3 |
| 15 | F6 | 601 | 45 | na | −1.5 | −6.7 | na | na | 4.9 |
| 16 | NTF6 | 541.4 | 31 | 21.5 | −2.5 | −9.1 | na | na | na |
| 17 | WNZ4R | 570.6 | 32 | 24.0 | −2.4 | −9.9 | na | na | na |
| 18 | NSA16B | 567.5 | 58.4 | 40.8 | −2.1 | −9.1 | −12.56 | na | 4.6±0.9 |
| 19 | JM247F | 540 | – | Falaj | −2.0 | −9.0 | na | na | na |
| Flow path 2 | | | | | | | | | |
| 20 | NSA17 | 565.3 | 95.4 | 56.5 | −2.8 | −9.5 | na | na | na |
| 21 | APM1 | 535.5 | 46 | 38.5 | −3.6 | −15.6 | na | na | na |
| 22 | APM6 | 498.3 | 46 | 33.0 | −2.5 | −9.5 | na | na | 3.7±1.0 |
| 23 | APM7 | 488.97 | 45.4 | 36.5 | −2.5 | −10.3 | na | na | na |
| 24 | APM10 | 446.1 | na | na | −1.9 | −8.3 | na | na | |
| 25 | APM15 | 443.1 | 23 | 11.5 | −2.3 | −8.9 | −14.23 | 90 | 5.9±1.3 |
| 26 | MN21 | 411.5 | 18 | 14.0 | −0.7 | −1.0 | na | na | na |
| 27 | MN24 | 432.6 | 30 | 22.0 | −2.3 | −10.3 | na | na | 3.8±0.6 |
| 28 | MN9-01 | 406.2 | 28.5 | 19.0 | −2.8 | −13.8 | na | na | na |
| 29 | JM243F | 565.3 | – | Falaj | −1.7 | −5.0 | na | na | na |
| 45 | MN16-01 | 490 | 28 | 22.5 | −1.3 | −12.2 | na | na | na |
| Flow path 3 | | | | | | | | | |
| 30 | APH15 | 606.17 | 36 | 24.5 | −2.1 | −5.7 | −14.68 | na | 6.5±1.4 |

 DOI 10.1007/s10040-004-0425-2

**Table 3** Continued

| | | | | | | | | | |
|---|---|---|---|---|---|---|---|---|---|
| 31 | APH01 | 609.9 | 29 | 17.0 | −1.9 | −3.6 | na | na | na |
| 32 | APH05 | 636.2 | 21 | 16.0 | −0.7 | −0.2 | na | na | na |
| 33 | APH04 | 622.36 | 29 | 17.0 | −1.8 | −5.3 | na | na | na |
| 34 | APH03 | 622.1 | 29 | 17.0 | −2.0 | −5.7 | na | na | na |
| 35 | APH08 | 468.9 | 21 | 10.0 | −0.3 | −0.2 | na | na | 4.2±0.9 |
| 36 | WHF03R | 450.95 | 34 | 19.0 | 0.5 | 2.1 | na | na | na |
| 37 | APH07 | 461.05 | 21 | 8.0 | −2.0 | −7.0 | na | na | na |
| 38 | NSA18B | 525 | 16 | 40.5 | −1.1 | −3.7 | −10.26 | na | 5.4±1.0 |
| 39 | WHF04R | 450.9 | 22 | 14.0 | −1.0 | −5.9 | na | na | 4.4±0.9 |
| 40 | APH02 | 609.61 | 36 | 24.0 | −2.1 | −4.9 | na | na | na |
| 41 | APH12 | 606.2 | 33 | 22.5 | −2.2 | −6.2 | na | na | na |
| Alluvial Aquifer: Southern Alluvial Plain | | | | | | | | | |
| 42 | MN5-01 | 351.2 | 20 | 14.0 | −1.8 | −9.4 | −14.10 | na | 4.1±0.6 |
| 43 | MN3-03 | 339.42 | 51 | 33.0 | −0.8 | −8.5 | −12.66 | na | 1.7±0.6 |
| 44 | MN8-01 | 368.89 | 28 | 15.0 | −1.8 | −8.2 | −13.60 | na | 2.4±0.6 |
| 46 | NWS4 | 385.6 | 25 | 15.5 | −2.1 | −9.9 | na | na | na |
| 47 | NWS10 | 382 | 42.5 | 27.5 | −2.5 | −14.1 | −13.81 | 88.1±1.18 | 3.3±1.0 |
| 48 | NWS15 | 370 | 31 | na | −2.0 | −11.9 | na | na | na |
| 49 | NWS6 | 365 | 37 | 25.0 | −1.9 | −10.4 | 13.61 | na | na |
| 50 | NWS5 | 380 | 61 | 38.0 | −2.4 | −12.0 | na | na | 4.5±1.0 |
| 51 | NSA33A | 321.1 | 52.5 | 44.5 | −2.2 | −12.0 | −14.71 | na | 0.6±0.6 |
| 52 | NSA35A | 321.1 | 59 | 43.5 | −2.0 | −9.6 | −12.20 | 72.7±3.0 | 0.7±0.9 |
| 53 | AG04 | 301.4 | 63.5 | 42.0 | −2.3 | −12.0 | na | na | na |
| 54 | AG33 | 301.3 | 71 | 50.5 | −2.0 | −10.4 | −11.71 | 61.5±2.2 | <0.8 |
| 55 | AG35 | 299.7 | 63 | 40.0 | −2.2 | −10.2 | −12.02 | 66.4±1.4 | <0.5 |
| 56 | WH10 | 304.7 | 35 | 19.5 | −2.0 | −11.4 | −12.40 | 73.5±1.6 | 2.3±1.0 |
| 57 | WH27 | 307.8 | 25 | 18.5 | −2.0 | −11.3 | na | na | 2.1 |
| 58 | WH21 | 303 | 29 | 16.5 | −1.8 | −11.1 | na | na | na |

### *Carbon isotope composition ($\delta^{13}C$)*

Measured $\delta^{13}C$ values in groundwater samples from the Hajar Supergroup aquifer of the Jabal Akhdar range from −6.1 to −8.5‰(Table 3) and are close to the $\delta^{13}C$ value of atmospheric $CO_2$. Groundwater in the Hajar Supergroup aquifer of the Adam Mountains is depleted in $^{13}C$ ($\delta^{13}C$=−9.8 and −10.6‰) compared to groundwater in the Jabal Akhdar, except for groundwater from the southern side of the Adam Mountains ($\delta^{13}C$=−6.7 and −8‰). The more depleted values are influenced by sulfate reduction as observed in groundwaters from the Adam Mountains. In the alluvial aquifer, groundwaters become irregularly depleted in $^{13}C$ ($\delta^{13}C$=−10.3 to −14.7‰) from the piedmont area to the Southern Alluvial Plain (Table 3). The lowest $\delta^{13}C$ values (−13.6 to −15.6‰) are recorded for groundwater from the ophiolite aquifer.

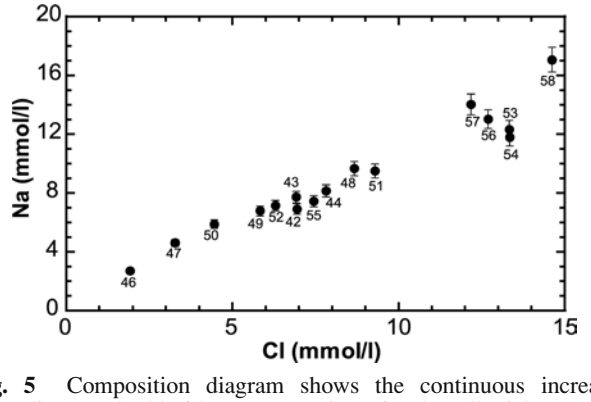


**Fig. 5** Composition diagram shows the continuous increase of sodium and chloride concentrations in the alluvial groundwater along the N–S flow path in the Southern Alluvial Plain (the *numbers* represent the sample location numbers, see Table 2)

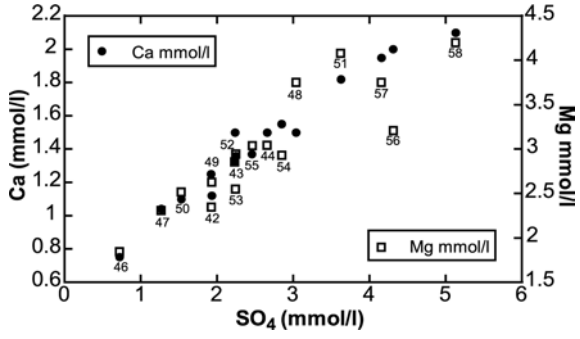


**Fig. 6** Ca and Mg vs. $SO_4$ composition plot illustrates the positive correlation of Ca and Mg with $SO_4$ along the N–S flow path in the Southern Alluvial Plain, suggesting the occurrence of dedolomitization reactions along the flow path in the alluvial aquifer (the *numbers* represent the sample location numbers, see Table 2)

 DOI 10.1007/s10040-004-0425-2

### Tritium

Tritium activities in $^{18}$O-depleted groundwater from the high-altitude recharge areas of the Jabal Akhdar range between 2.8 and 4.2 TU and decrease to values around the detection limit (<0.5 TU) in the less $^{18}$O-depleted groundwaters sampled in the low-altitude areas (<1,200 m) of the Jabal Akhdar (Table 3). Tritium activities of modern rainfall in Oman vary between about 5–10 TU (Weyhenmeyer 2000). This indicates that the high-altitude groundwaters are essentially modern in origin and that the residence time of such groundwater in the fractured and karstified limestones and dolomites is in the order of a few decades at maximum.

Groundwaters from wells in the low-altitude areas of the Jabal Akhdar and the piedmont area of the alluvial plain have tritium activities between 3.7 and 7.8 TU. Compared to the high-altitude groundwaters from the Jabal Akhdar, these high activities indicate a large portion of recent, local infiltration along the foothills, which is consistent with the stable isotope composition of these waters being more enriched in $^{18}$O.

In the Southern Alluvial Plain the tritium activity in the groundwater shows a heterogeneous spatial distribution and ranges from 4.5 TU to below detection limit (<0.5 TU) in the southernmost part. Highest tritium activities are recorded in shallow groundwater close to the main wadi channels. While the tritium activity generally decreases along the main flowpaths from north to south, it also decreases laterally with increasing distance from the main wadi channels as it has already been observed previously by Cansult/Gartner and Lee (1986) and Clark (1987).

Groundwater sampled from deep wells in the Hajar Supergroup aquifer of the eastern Adam Mountains (Jabal Madmar) is tritium-free, indicating that no modern recharge component contributes to these waters (Table 3). This contrasts the measurable tritium activities between 0.8 to 10 TU of shallow groundwater from the western Adam Mountains (Jabal Salakh and Jabal Nahdah) reported by Cansult/Gartner and Lee (1986).

### Carbon-14

Similar to the tritium activities, radiocarbon activities ($^{14}$C) in groundwater samples from the Hajar Supergroup aquifer decrease from 54.1 to 35.4 pmc from the high to the low altitude areas of the Jabal Akhdar (Table 3). Groundwater from the alluvial aquifer has higher $^{14}$C activities between 90 and 61.5 pmc, which correlate with the tritium activities of the same samples. The tritium-free deep groundwaters from the eastern Adam Mountains have low $^{14}$C activities between 40.9 and 0 pmc (Table 3).

## Discussion

Based on the hydrochemical, isotopic and hydrogeological data five main regions with different groundwater evolution are recognized: (1) mountainous areas of the Jabal Akhdar with direct recharge of infiltrating precipitation, (2) ophiolitic foothills with mainly direct recharge of infiltrating rain, (3) alluvial piedmont area with direct recharge of rain water and/or indirect recharge by surface runoff from the adjacent mountainous areas (Jabal Akhdar and/or ophiolite), (4) Southern Alluvial Plain, with direct recharge of rain and surface runoff from the plain and/or indirect recharge (subsurface inflow) from the alluvial piedmont, (5) Eastern Adam Mountains, with no dominant modern-day recharge. To quantitatively evaluate the origin and geochemical evolution of the different groundwater types in the Halfayn alluvial aquifer system, the environmental isotope data are combined with geochemical modeling.

### Recharge areas and moisture sources

Groundwater sampled above 1,550 m in the high-altitude regions of the Jabal Akhdar is significantly depleted in $^{18}$O and $^{2}$H ($\delta^{18}$O‰=−3.4±0.3‰, $\delta^{2}$H=−15.5±2.4‰; $n$=5) compared to that in the foothills and alluvial plain. This depleted isotope signature is attributed to the altitude effect on precipitation. An altitude effect on the stable isotope composition of water in northern Oman has already been described in previous studies (Cansult/Gartner and Lee 1986; Clark 1987; Macumber 1997, 1998; Weyhenmeyer et al. 2002). Groundwater in the low-lying area of the Jabal Akhdar between about 600 and 1,200 m of altitude has average $\delta^{18}$O and $\delta^{2}$H values of −2.5±0.6‰and −8.2±4.8‰($n$=7), respectively. If the groundwater in this area would be local recharge from the same precipitation event(s) as in the high-altitudes, its $\delta^{18}$O would become about −1.7‰based on average altitudes of 1,900 m (high-altitudes) and 800 m (low-altitude) and on the altitude effect of 0.15‰per 100 m as observed by Weyhenmeyer et al. (2002). The difference in isotopic composition between groundwaters from the high- and low-altitude areas can hardly be explained by evaporational effects because of their similar Cl concentrations (high-altitude: 25.7±6.3 mg/l Cl, $n$=5; low-altitude: 30.2±7.4 mg/l Cl, $n$=7). These average Cl contents suggest an evaporation of about 15%, which results in values for $\delta^{18}$O and $\delta^{2}$H in the remaining water of −2.0 and −4.0‰, respectively, using the Rayleigh distillation relationship and an average temperature of 30°C for the fractionation factors. The stable isotope and Cl data thus indicate that the groundwaters in the low-altitude area represent a mixture of high-altitude and local recharge.

In the piedmont alluvial aquifer the altitude effect would result in a similar difference of more than 1‰ between the measured and altitude-corrected $\delta^{18}$O values using the relationship of Weyhenmeyer et al. (2002). The somewhat higher Cl concentrations in these groundwaters (average of 55.7±15.6 mg/l Cl, $n$=6, and 37.3±13.0 mg/l Cl, $n$=11, for flow path 1 and 2, respectively) compared to the Jabal Akhdar groundwaters could suggest an enrichment by evaporation of about 54% for the groundwaters of flow path 1 (Wadi Abyadh) and 31% for those of flow path 2 (Wadi

 DOI 10.1007/s10040-004-0425-2

M'uaydin). Using the Rayleigh distillation relationship it can be shown, however, that such a high amount of evaporation would result in an isotopic composition of the remaining water fraction that is too enriched in the heavy isotopes $^{18}O$ and $^{2}H$ ($\delta^{18}O > -0.2‰$ and $\delta^{2}H > +9.8‰$ at 31% evaporation) compared to the measured values. Thus, it can be concluded that also the piedmont alluvial groundwaters along flow path 1 and 2 represent a mixture of high-altitude water and local infiltration. Such a scenario is also consistent with the available $^{3}H$ and $^{14}C$ data, which are identical or even higher (i.e. shorter average residence time) than those of the high-altitude Jabal Akhdar waters. The existence of a locally infiltrated component in flow path 1 and flow path 2 is further supported by the lower $\delta^{13}C$ values in these waters, which are derived from the dissolution of secondary, $^{13}C$ depleted carbonate cement in the wadi channels (see below). The relatively large spread in the data between individual sampling locations and the lack of monitoring data over several years, however, do not allow the quantification of the individual proportions.

A different picture arises for the groundwater of flow path 3 (Wadi Halfayn) and the ophiolite aquifer. For flow path 3 the altitude effect could in fact explain the enrichment in $^{18}O$ within the overall error ( $\delta^{18}O_{measured} = -1.4 \pm 0.9‰$, $n$=12, and $\delta^{18}O_{alt.-corrected} \approx -1.3‰$). However, the average Cl concentration in the groundwaters of flow path 3 is significantly higher than in the Jabal Akhdar groundwaters although a large spread is observed (70.9±62.8 mg/l Cl). Obviously, evaporation of water derived from the Jabal Akhdar cannot explain these Cl concentrations as this would result in an isotopic composition that is much more enriched in the heavy isotopes than observed. Based on the isotope data and the prevailing hydraulic gradients in upstream Wadi Halfayn, a three component mixture of water derived from the Jabal Akhdar, the ophiolite aquifer and local recharge is proposed for flow path 3 groundwater and will be explored by mixing calculations below. For the ophiolite aquifer the altitude effect would even result in a too low $\delta^{18}O$ value ( $\delta^{18}O_{measured} = -0.9 \pm 0.3‰$, $n$=8, and $\delta^{18}O_{alt.-corrected} \approx -1.2‰$) indicating that additional evaporation appears to take place in agreement with the increased Cl contents (113.0±75.2 mg/l Cl). Besides, the major moisture source appears to be different for these groundwaters (see below). In the $\delta^{18}O$–$\delta^{2}H$ diagram (Fig. 7) the trend described by the isotopic composition of Jabal Akhdar groundwater differs from that of groundwater from the other aquifers. Together with the above evaluation of the possible effects of altitude and evaporation on the isotopic composition this also indicates differences in the major moisture sources. For the evaluation of the sources, the groundwater isotopic data can be compared to meteoric water lines derived from precipitation data. There exist numerous studies on the isotopic composition of precipitation in Oman (Cansult/Gartner and Lee 1986; Stanger 1986; Clark et al. 1987; Wushiki 1991; Macumber et al. 1995, 1997; Macumber 1998, 2003; Weyhenmeyer et al. 2002) several of them resulting in the definition of meteoric water lines for different areas in Oman.

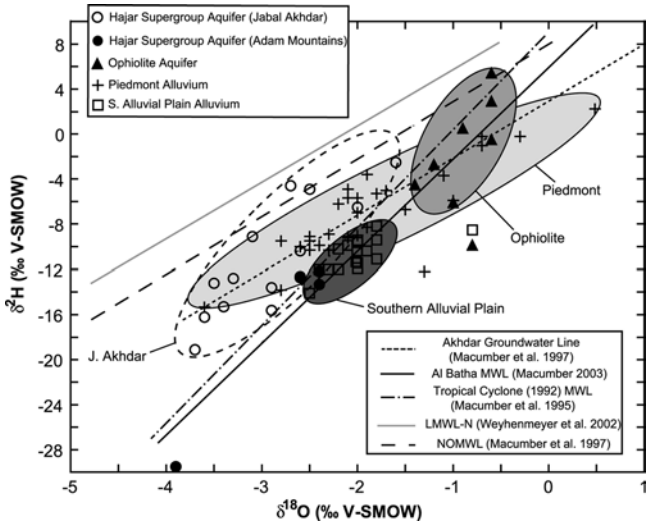


**Fig. 7** $\delta^{18}O$–$\delta^{2}H$ plot of all groundwater samples from the different aquifers together with the most recent published local meteoric water lines of Oman. The plot shows the differences in the groundwater isotopic composition between the individual aquifers in relation to the local meteoric water lines, whereas the differences were taken as an indication for differences in the recharge altitude, evaporation effects and moisture sources

The review of a large dataset by Macumber et al. (1997) and Macumber (1998) resulted in a new meteoric water line for northern Oman, the so-called Northern Oman Meteoric Water Line (NOMWL; $\delta^{2}H = 5.1\delta^{18}O + 8.0$. Based on a dataset from 1995 to 1998, Weyhenmeyer et al. (2002) defined a local meteoric water line for the Batinah coastal plain in northern Oman, the local meteoric water line-northern moisture sources (LMWL-N; $\delta^{2}H = 5.0\delta^{18}O + 10.7$). This water line represents the isotopic relationship of rainfall from a northern (frontal) source only, whereas the NOMWL by Macumber (op. cit.) includes data from all different precipitation sources in northern Oman. The similarity between these two water lines reveals, however, that the majority of rainfall in the Jabal Akhdar Mountains and the adjacent coastal plains of northern Oman is from a northern (frontal) source. The two meteoric water lines are further similar to those established for southwestern Israel ( $\delta^{2}H = 5.8\delta^{18}O + 8.6$; Nativ et al. 1995) and Bahrain ( $\delta^{2}H = 5.3\delta^{18}O + 9.2$; Rozanski and Araguás-Araguás 1992), suggesting a similar origin of water vapor and its transport history (Weyhenmeyer et al. 2002; Macumber 2003).

Macumber et al. (1995) also defined a local meteoric water line in Central Oman for tropical cyclones arriving from the south ( $\delta^{2}H = 8.7\delta^{18}O + 9.1$) based on the storm event during the passage of cyclone O6-A in central Oman in 1992. Rainfall from another heavy storm event in northern Oman in July 1995 was used by Macumber (2003) to define the so-called Al Batha line ( $\delta^{2}H = 8.1\delta^{18}O + 5.8$). This storm event appears to be more of an example of a large, southern low-pressure frontal system that reached northern Oman because it was not registered as a tropical cyclone.

As shown in Fig. 7, the isotopic composition of the groundwater samples from the present study plot to the


DOI 10.1007/s10040-004-0425-2

right of the NOMWL of Macumber et al. (1997) and the LMWL-N of Weyhenmeyer et al. (2002), which describe the typical northern moisture source. Groundwater from the Hajar Supergroup aquifer in the Jabal Akhdar plots in between the meteoric water lines given for typical northern and southern moisture sources and are thus interpreted as mixtures of these sources. For groundwater of the piedmont alluvial aquifer a linear regression through all data provides the local groundwater line ( $\delta^2H = 4.34\delta^{18}O + 1.27$, $R^2$=0.91) for this area. This local groundwater line is similar in slope and intercept to the Akhdar Water Line ( $\delta^2H = 5.1\delta^{18}O + 3.0$; Macumber et al. 1997), which is based on 50 groundwater samples from springs and aflaj of the Jabal Akhdar. The present samples support the interpretation of this Akhdar Line by Macumber et al. (1997) stating that it reflects the influence of a high altitude recharge source from the Jabal Akhdar with a dominantly northern moisture source to the groundwater in the piedmont alluvium.

The linear regression lines through the data points of the ophiolite and the Southern Alluvial Plain aquifer approximate the Al Batha Line and the water line derived from the tropical cyclone of 1992 (Fig. 7). This suggests that the dominant moisture source of these groundwaters comes from the south. Similarly, the isotopic compositions of groundwaters from the Hajar Supergroup aquifer of the Adam Mountains plot along the water line derived from the tropical cyclone of 1992 demonstrating the dominant influence of a southern moisture source in the Hajar Supergroup aquifer of the Adam Mountains.

## Geochemical evolution of groundwater

As a function of time, groundwater tends to attain equilibrium with the mineralogy of the aquifer rock. Information about the present equilibrium state of an individual groundwater is obtained from the mineral saturation indices (SI), which describe the tendency of a water to either dissolve (negative SI) or precipitate (positive SI) a mineral. To quantitatively support or reject proposed evolutionary pathways for the groundwaters from the Hajar Supergroup aquifer of the Jabal Akhdar to the Southern Alluvial Plain aquifer mass balance, mass transfer and mixing calculations including isotopic data are applied and compared to the calculated mineral saturation state of the groundwater in question.

Using the pH values measured in the field, the speciation calculations reveal for most groundwaters an oversaturation with respect to calcite. This is geochemically unlikely because in calcite-bearing rocks equilibrium with calcite is commonly established and maintained within days (Pearson et al. 1978). Based on the tritium contents of the groundwaters, their residence time is in the order of at least a few years and thus equilibrium with respect to calcite can be expected for all these groundwaters. There are mainly two reasons that might account for the calculated calcite oversaturation: Firstly, outgassing of $CO_2$ from the groundwater might have occurred in the sampling system used, which was open to the atmosphere. As a consequence a too high pH value is measured that is no longer representative for in-situ conditions and results in an apparent calcite oversaturation for the groundwater. Obviously, degassing of $CO_2$ from a water sample will change the total inorganic carbon (TIC) content of the water and thus prevent accurate mass balance calculations and corrections of the measured $^{14}C$ data. Secondly, the calculated calcite oversaturation might be true and due to the inhibition of calcite precipitation. Dissolved Mg is well-known to act as an inhibitor of calcite precipitation (Berner 1975; Plummer et al. 1979) and a calculated $S_{calcite}$ of up to 0.3 in groundwater with a Mg/Ca ratio similar to that of seawater (about 5) might in fact represent in-situ conditions (Appelo and Postma 1996).

Groundwater with Mg/Ca ratios around 5 is only found in the ophiolite aquifer (Table 2). In these groundwaters a certain inhibition of calcite precipitation might in fact occur. However, $SI_{calcite}$ values calculated with the pH value measured in the field are either between 0 and 0.15 (i.e. calcite equilibrium) or they are higher than 0.4. In these latter samples degassing of $CO_2$ was observed during sampling, which justifies the correction of the TIC content and the pH value of these analyses to calcite equilibrium. Similarly, the correction of the water analyses to calcite equilibrium seems also justified for groundwater samples along flow path 3 and the Southern Alluvial Plain with elevated Mg/Ca ratios between 1.2 and 3.1 (Table 2) and where degassing of $CO_2$ was frequently observed during sampling.

### *Hajar Supergroup aquifer of the Jabal Akhdar*

At calcite equilibrium groundwater from the Hajar Supergroup aquifer of the Jabal Akhdar is in equilibrium with dolomite, except for two spring waters, which are undersaturated with respect to dolomite (Table 4). All Jabal Akhdar groundwaters are undersaturated with respect to chalcedony, which can be used as a proxi for quartz in natural groundwaters (Rimstidt 1997).

The chemical evolution of the Jabal Akhdar groundwaters can be explained by direct infiltration of rainfall with subsequent uptake of soil-$CO_2$ resulting in the dissolution of calcite and dolomite, and the oxidation of pyrite induced by the dissolved oxygen in rainwater. The congruent dissolution of calcite and dolomite is then described as:

$$CaCO_{3(s)} + CO_2 + H_2O = Ca^{2+} + 2HCO_3^- \quad (1)$$

$$CaMg(CO_3)_{2(s)} + 2CO_2 + 2H_2O = Ca^{2+} + Mg^{2+} + 4HCO_3^- \quad (2)$$

The $CO_2$ in these reactions is derived from the atmosphere and, where present, from the soil cover. In general, dissolution of dolomite is slower than that of calcite and may often take place in significant amounts only below the water table under closed system conditions (Busenberg and Plummer 1982; Clark and Fritz 1997).

The molar Mg/Ca ratios in groundwater samples from springs and boreholes from the Hajar Supergroup aquifer of the Jabal Akhdar are either below or around one (Table 2).

 DOI 10.1007/s10040-004-0425-2

**Table 4** Calculated saturation indices (calcite saturation is assumed) of groundwater samples from the different aquifers

| No | Well ID | Calcite | Log $P_{CO_2}$ | Dolomite | Gypsum | Magnesite | Brucite | Quartz | Chalcedony |
|---|---|---|---|---|---|---|---|---|---|
| Hajar Super Group Aquifer: Jabal Akhdar | | | | | | | | | |
| 1 | JA05 | 0 | −1.66 | 0.09 | | | | 0.28 | −0.16 |
| 2 | JA17 | 0 | −1.78 | 0.05 | | | | 0.32 | −0.11 |
| 3 | SP03 | −0.11 | −1.61 | −0.92 | | | | 0.32 | −0.11 |
| 4 | SP04 | 0 | −2.07 | −0.42 | | | | na | na |
| 5 | SP05 | 0 | −1.9 | −0.08 | | | | 0.17 | −0.24 |
| 6 | SP06 | 0 | −1.99 | 0.16 | | | | na | na |
| 7 | SP07 | 0 | −2.01 | −0.14 | | | | 0.18 | −0.26 |
| 8 | SP08 | 0 | −1.58 | −0.07 | | | | 0.23 | −0.2 |
| 9 | SP09 | 0 | −2.39 | 0.18 | | | | na | na |
| 10 | SP10 | 0 | −2.55 | 0 | | | | na | na |
| 11 | NSA32 | 0 | −2.04 | 0.07 | | | | 0.19 | −0.21 |
| 12 | NSA09 | 0 | −1.52 | −0.02 | | | | 0.22 | −0.19 |
| 73 | JA10S | 0 | −1.9 | 0.16 | | | | 0.21 | −0.19 |
| Hajar Super Group Aquifer: Adam Mountains | | | | | | | | | |
| 68 | AA01 | 0 | −1.65 | 0.37 | −1.1 | | | 0.48 | 0.09 |
| 69 | ADM03 | 0 | −1.6 | 0.29 | −1.15 | | | 0.39 | 0.01 |
| 71 | ADM01 | 0 | −2.03 | 0.1 | −1.95 | | | 0.26 | −0.13 |
| 74 | AA07 | 0 | −1.71 | 0.2 | −1.12 | | | 0.44 | 0.05 |
| Ophiolite aquifer | | | | | | | | | |
| 59 | WHF09R | 0 | −2.57 | 0.84 | | 0.25 | −3.46 | na | na |
| 60 | SHD11R | 0 | −2.32 | 0.76 | | 0.16 | −3.73 | 0.56 | 0.16 |
| 61 | F2204 | 0 | −3.67 | 0.95 | | 0.36 | −2.44 | na | na |
| 62 | F2221 | 0 | −2.15 | 0.98 | | 0.39 | −3.95 | na | na |
| 63 | F0474 | 0 | −2.36 | 0.86 | | 0.26 | −3.67 | na | na |
| 64 | F0473 | 0 | −2.58 | 1.04 | | 0.45 | −3.42 | na | na |
| 66 | WNZ21A | −0.4 | −1.58 | −0.11 | | −0.31 | −4.98 | 0.56 | 0.16 |
| 67 | WNZ08 | 0 | −1.45 | 0.75 | | 0.15 | −4.61 | 0.65 | 0.25 |
| Alluvial Aquifer: Piedmont | | | | | | | | | |
| Flow path 1 | | | | | | | | | |
| 13 | NSA15 | 0 | −2.13 | −0.06 | −2.1 | −0.65 | −4.85 | 0.19 | −0.21 |
| 14 | F5 | 0 | −1.75 | 0.01 | −1.95 | −0.58 | −5.14 | 0.31 | −0.09 |
| 15 | F6 | 0 | −1.89 | −0.06 | −2.01 | −0.65 | −5.25 | 0.24 | −0.17 |
| 16 | NTF6 | 0 | −1.92 | 0.13 | −2.13 | −0.47 | −4.79 | 0.45 | 0.05 |
| 17 | WNZ4R | 0 | −1.45 | −0.02 | −1.84 | −0.62 | −5.47 | 0.48 | 0.08 |
| 18 | NSA16B | 0 | −1.81 | 0.04 | −2.15 | −0.56 | −5.06 | 0.35 | −0.05 |
| 19 | JM247F | 0 | −2.02 | 0.07 | −2.26 | −0.52 | −4.86 | 0.39 | −0.02 |
| Flow path 2 | | | | | | | | | |
| 20 | NSA17 | 0 | −2.28 | −0.04 | −2.05 | −0.63 | −4.72 | 0.3 | −0.1 |
| 21 | APM1 | 0 | −2.4 | 0.2 | −2.22 | −0.39 | −4.32 | na | na |
| 22 | APM6 | 0 | −1.87 | 0.17 | −2.03 | −0.46 | −4.88 | na | na |
| 23 | APM7 | 0 | −1.81 | 0.01 | −2.01 | −0.59 | −5.07 | 0.29 | −0.12 |
| 24 | APM10 | 0 | −2.22 | 0.35 | −2.23 | −0.24 | −4.27 | 0.57 | 0.17 |
| 25 | APM15 | 0 | −1.73 | 0.21 | −1.94 | −0.38 | −4.99 | 0.57 | 0.16 |
| 26 | MN21 | 0 | −2.02 | 0.08 | −2.08 | −0.52 | −4.72 | 0.47 | 0.07 |
| 27 | MN24 | −0.1 | −1.68 | −0.09 | −1.88 | −0.59 | −5.19 | 0.47 | 0.07 |
| 28 | MN9-01 | −0.33 | −1.42 | −0.3 | −1.97 | −0.57 | −5.33 | 0.59 | 0.2 |
| 29 | JM243F | 0 | −1.90 | 0.02 | −1.98 | −0.58 | −5.1 | 0.36 | −0.05 |
| 45 | MN16-01 | −0.64 | −1.63 | −0.66 | −2.27 | −0.62 | −5.19 | 0.52 | 0.12 |
| Flow path 3 | | | | | | | | | |
| 30 | APH15 | 0 | −1.75 | 0.35 | −2.45 | −0.24 | −4.83 | na | na |
| 31 | APH1 | 0 | −2.06 | 0.46 | −2.66 | −0.14 | −4.41 | na | na |
| 32 | APH5 | 0 | −2.34 | 0.25 | −2.78 | −0.34 | −4.48 | 0.45 | 0.03 |
| 33 | APH4 | 0 | −2.04 | 0.36 | −2.68 | −0.23 | −4.59 | 0.55 | 0.14 |

 DOI 10.1007/s10040-004-0425-2

**Table 4** Continued

| | | | | | | | | | |
|---|---|---|---|---|---|---|---|---|---|
| 34 | APH3 | 0 | −1.79 | 0.45 | −2.9 | −0.15 | −4.73 | na | na |
| 35 | APH8 | 0 | −1.93 | 0.71 | −2.09 | 0.12 | −4.25 | na | na |
| 36 | WHF3R | 0 | −2 | 0.58 | −2.01 | −0.01 | −4.33 | 0.5 | 0.09 |
| 37 | APH07 | 0 | −2.1 | 0.54 | −2.49 | −0.06 | −4.3 | na | na |
| 38 | NSA18B | 0 | −1.64 | 0.73 | −1.99 | 0.14 | −4.59 | 0.62 | 0.21 |
| 39 | WHF4R | 0 | −1.94 | 0.71 | −2.01 | 0.11 | −4.18 | na | na |
| 40 | APH02 | 0 | −1.91 | 0.4 | −2.72 | −0.18 | −4.63 | 0.51 | 0.1 |
| 41 | APH12 | 0 | −1.82 | 0.28 | −2.45 | −0.31 | −4.84 | 0.44 | 0.04 |
| Alluvial Aquifer Southern Alluvial Plain | | | | | | | | | |
| 42 | MN5-01 | −0.06 | −1.93 | 0.4 | −1.5 | −0.14 | −4.4 | 0.6 | 0.21 |
| 43 | MN3-03 | 0 | −1.84 | 0.56 | −1.87 | −0.03 | −4.45 | 0.66 | 0.26 |
| 44 | MN8-01 | −0.13 | −1.6 | 0.27 | −1.51 | −0.2 | −4.77 | 0.62 | 0.22 |
| 46 | NWS4 | 0 | −2.06 | 0.63 | −2.19 | 0.03 | −4.08 | 0.58 | 0.18 |
| 47 | NWS10 | 0 | −1.87 | 0.56 | −1.87 | −0.03 | −4.45 | 0.43 | 0.03 |
| 48 | NWS15 | 0 | −1.78 | 0.61 | −1.49 | 0.02 | −4.45 | 0.7 | 0.3 |
| 49 | NWS6 | 0 | −1.92 | 0.59 | −1.72 | −0.01 | −4.33 | 0.6 | 0.2 |
| 50 | NWS5 | 0 | −1.85 | 0.57 | −1.8 | −0.02 | −4.45 | 0.62 | 0.22 |
| 51 | NSA33A | 0 | −1.74 | 0.57 | −1.35 | −0.03 | −4.5 | 0.68 | 0.28 |
| 52 | NSA35A | 0 | −1.81 | 0.52 | −1.61 | −0.05 | −4.45 | 0.63 | 0.23 |
| 53 | AG04 | −0.04 | −2.08 | 0.43 | −1.58 | −0.16 | −4.3 | 0.54 | 0.14 |
| 54 | AG33 | 0 | −2.01 | 0.5 | −1.49 | −0.1 | −4.27 | 0.52 | 0.12 |
| 55 | AG35 | 0 | −1.83 | 0.57 | −1.57 | −0.02 | −4.36 | 0.62 | 0.22 |
| 56 | WH10 | 0 | −1.71 | 0.42 | −1.25 | −0.18 | −4.69 | 0.65 | 0.25 |
| 57 | WH27 | 0 | −1.68 | 0.5 | −1.29 | −0.1 | −4.66 | 0.64 | 0.24 |
| 58 | WH21 | 0 | −1.61 | 0.51 | −1.21 | −0.08 | −4.69 | 0.68 | 0.28 |

The calculations were done with PHREEQC 2, using the WATEQ4f data base

The increase in the sulfate concentration of groundwater from the Jabal Akhdar (0.15–1.16 mmol/l) compared to the average sulfate concentration in rainfall (0.12 mmol/l; Stanger 1986) is attributed to small amounts of pyrite oxidation. Pyrite is a common mineral phase within the micritic matrix of organic-rich, shaly limestones in the Permian to Cretaceous carbonate rocks of the Hajar Supergroup aquifer (Rathmayr 2000). The acidity produced by pyrite oxidation will additionally promote calcite dissolution according to:

$$CaCO_{3(s)} + H^+ = Ca^{2+} + HCO_3^- \quad (3)$$

The calculated mass transfer and isotopic composition of TIC ($\delta^{13}C_{TIC}$) is presented in Table 5. The isotopic data used in these calculations for calcite and dolomite of the Hajar Supergroup sediments and soil-$CO_2$ are taken from the literature and given in Table 6. The measured $\delta^{13}C_{TIC}$ values are well reproduced by the calculations using the appropriate $\delta^{13}C$ value for soil-$CO_2$ (cf. Table 6) and support the proposed geochemical evolution. Differences exist, however, in the calculation of the dilution of the $^{14}C$ activity by $^{14}C$-free carbon from mineral dissolution. For the high-altitude waters of the Jabal Akhdar (samples JA05 and JA17) the mass balance calculations reveal that the decrease of the $^{14}C$ activity in rain is almost entirely made by dilution with $^{14}C$-free carbon from the dissolution of calcite and dolomite. The average $^{14}C$-residence time of these waters is calculated to be less than 50 years in agreement with the measured $^3H$ activities (Table 2). As shown above, the low-altitude waters (sample NSA09 and NSA32) represent a mixture of high-altitude water and local infiltration, which inhibits the derivation of a $^{14}C$-residence time. In combination with the $^3H$ activity one component appears to be older than 50 years, while the other must be recent. It is important to recognize that $^{14}C$ activities of <54 pmc in the recharge area of the Jabal Akhdar are significantly lower compared to those measured in groundwater from the down-gradient alluvial aquifer (61.5–90 pmc). This bears its consequences on the origin and evolution of these alluvial groundwaters.

### *Ophiolite aquifer*

Groundwaters from the ophiolite aquifer display a large variability in total mineralization (580±318 mg/l TDS) and Cl concentrations (113.0±75.2 mg/l Cl) indicating different degrees of geochemical evolution. All ophiolite groundwaters were sampled from strongly serpentinized peridotites where contact with the primary mineralogy of the rocks is limited. This is indicated by the high molar $Mg^{2+}/H_4SiO_4$ (9.2) and $Ca^{2+}/H_4SiO_4$ (2.3) ratios in the groundwaters, which differ significantly from the primary mineral assemblage in the rock ($Mg^{2+}/SiO_2$ =1.63, $Ca^{2+}/SiO_2$ =0.007), and which suggest that primary mineral dissolution is not a dominant process (Stanger 1986). Therefore, the chemistry and the evolution of the shallow ophiolite groundwater differs from that of the high-pH

 DOI 10.1007/s10040-004-0425-2

**Table 5** Results of chemical and isotope mass balance calculations to evaluate $^{14}C$ residence times for selected groundwater samples from the Hajar Supergroup aquifer in the Jabal Akhdar

| Initial | Final | Mass transfer (mmol/kg $H_2O$) Calcite | Dolomite | $CO_2$ (g) | $\delta^{13}C$ (‰) | $^{14}C$ (pmc) | Residence time (years)[a] |
|---|---|---|---|---|---|---|---|
| High-altitude groundwater | | | | | | | |
| Rain | JA05 | 0.18 | 1.53 | 3.75 | −9.1 | 54.3 | <50 |
| Rain | JA17 | 0.11 | 1.45 | 2.26 | −8.5 | 46.8 | <50 |
| Low-altitude groundwater | | | | | | | |
| Rain | NSA09 | 0.77 | 1.36 | 2.13 | −7.6 | 42.0 | Component 1: <50 |
| | | | | | | | Component 2: >50 |
| Rain | NSA32 | 0.18 | 1.31 | 0.95 | −6.6 | 39.4 | Component 1: <50 |
| | | | | | | | Component 2: >50 |

Positive numbers in the chemical mass transfer indicate dissolution of a mineral phase. The calculated $\delta^{13}C$ values (‰PDB) match with those measured for the high- and low-altitude groundwaters using the corresponding soil-$CO_2$ values (cf. Table 6). Carbon-14 residence times can be calculated for the high-altitude waters whereas the low-altitude waters represent mixtures of different waters (see text)

[a]Includes analytical uncertainty and uncertainty in the initial $^{14}C$ input values (100–110 pmc)

**Table 6** Selected isotopic properties of phases included in the mass transfer calculations

| Phases | $\delta^{13}C$ (‰) | $^{14}C$ (pmc) | Reference |
|---|---|---|---|
| Calcite | 0.0±2.0 | 0 | Hoefs (1997) |
| Dolomite | 0±2.0 | 0 | Hoefs (1997) |
| $CO_2$(g)soil high-altitude | −15±2.0 | 100–110 | Clark (1987) |
| $CO_2$(g)soil low-altitude | −20±2.0 | 100–110 | Cansult/Gartner and Lee (1986) |
| Magnesite | −7.8±1.1 | 0 | C.E. Weyhenmeyer (2003, personal communication) |
| High-Mg-calcite cement (secondary)[a] | −6.5 | 0 | Burns and Matter (1995) |
| Dolomite cement (secondary)[a] | −6.9±1.8 | 0 | Burns and Matter (1995) |
| Calcite cement (secondary)[a] | −5.6±1.5 | 0 | Burns and Matter (1995) |
| Brucite, gypsum, halite quartz | | | |

[a]Including only measurements from the south of the Oman Mountains (see Burns and Matter 1995)

groundwater (pH between 11 and 12) of the chemical Mg–OH and Ca–OH type that evolves at greater depth in the ophiolite and is found elsewhere in the area (Neal and Stanger 1985; Clark 1987; Clark and Fontes 1990). The high magnesium concentrations in the shallow, Mg–(Na)–$HCO_3$–(Cl) type groundwaters of the ophiolite aquifer result at calcite equilibrium in an oversaturation of the waters with respect to dolomite and magnesite. They are further oversaturated with respect to chalcedony (as a proxi for quartz, see above) and undersaturated with respect to brucite.

The chemical evolution of surface water and shallow groundwater in the ophiolites is discussed by Neal and Stanger (1985) and Stanger (1986). According to these authors, the Mg–(Na)–$HCO_3$–(Cl) type waters are the result of weathering and evaporative processes in a system open to the atmosphere. The high magnesium and bicarbonate concentrations are attributed to the dissolution of near-surface brucite according to:

$$Mg(OH)_{2(s)} + 2CO_2 = Mg^{2+} + 2HCO_3^- \quad (4)$$

The high solubility of brucite accounts for the generation of Mg–$HCO_3$ type surface and shallow groundwater in completely serpentinized rocks, which is consistent with the low brucite content in these strongly weathered rocks (Neal and Stanger 1985). Neal and Stanger (1985) further postulated that continuous brucite dissolution in the shallow aquifer will lead to the formation of secondary magnesite according to:

$$Mg(OH)_{2(s)} + Mg^{2+} + 2HCO_3^- = 2MgCO_{3(s)} + 2H_2O \quad (5)$$

Magnesite veins of some millimeters to decimeters in thickness are abundant in the ultramafics and the formation of such magnesite is in agreement with the magnesite supersaturation calculated for the shallow ophiolite groundwaters of the present study. In addition, the carbonate isotopic composition ($\delta^{18}O$, $\delta^{13}C$) of magnesite from such veins confirms a formation under low-temperature conditions from a meteoric fluid (C.E. Weyhenmeyer personal communication 2003).

### *Piedmont alluvial aquifer*

The general chemical composition, total mineralization and Ca/Mg ratios of groundwater along flow paths 1 and 2 in the piedmont alluvial aquifer are similar to those of the Hajar Supergroup aquifer of the Jabal Akhdar (Table 2, Figs. 3 and 4). These latter groundwaters are in equilibrium with respect to calcite and dolomite and close to or at equilibrium with respect to chalcedony, but undersaturated with respect to all other mineral phases (Table 4). This indicates that their general chemical evolution is essentially

 DOI 10.1007/s10040-004-0425-2

the same as for groundwater from the Jabal Akhdar. This is not surprising because the sediments of Wadi Abyadh (flow path 1) and Wadi Mu'aydin (flow path 2) are essentially made of debris from the Jabal Akhdar mountains. The only difference is the cementation of the wadi sediments with secondary calcite and dolomite that has about 6–9‰lower $\delta^{13}C$ values (Burns and Matter 1995) compared to the mainly marine Hajar Supergroup carbonates.

Based on their stable isotope composition ($\delta^{18}O$, $\delta^{2}H$) and the Cl concentration, these groundwaters represent a mixture of high-altitude Jabal Akhdar water and local infiltration. The $\delta^{13}C_{TIC}$ is significantly more negative (<−12.5‰) compared to these of the Jabal Akhdar groundwater (−6.2 to −8.5‰). These negative $\delta^{13}C_{TIC}$ values therefore support a local recharge component, which will dissolve secondary carbonate cement during its infiltration into the underground until chemical equilibrium is attained. In contrast, groundwaters along flow path 3 (Wadi Halfayn) are oversaturated with dolomite and commonly undersaturated with magnesite (Table 4). The Mg/Ca ratio of these groundwaters (2.0±0.8, $n$=12) is higher compared to that of flow path 1 (0.6±0.1, $n$=6) and flow path 2 (0.9±0.3, $n$=11). Groundwater at equilibrium with calcite and dolomite has a Mg/Ca ratio of about 0.8 indicating an additional Mg source in the groundwaters along flow path 3.

The following potential sources for recharge to the alluvial aquifer in the piedmont of Wadi Halfayn can be defined based on the hydrogeological setting: (1) direct infiltration of rainfall, (2) infiltration of surface runoff from the Jabal Akhdar along active wadi channels, (3) groundwater from the adjacent Hajar Supergroup aquifer, and (4) surface runoff and/or shallow groundwater from the adjacent ophiolite aquifer. Mixing calculations using $\delta^{18}O$ and Cl as mixing variables and mean chemical compositions of the four potential sources (Table 7) reveal that the chemical and stable isotopic composition of the average flow path 3 groundwater (target alluvium water in Table 7) is the result of a three component mixture of rain (∼10%), surface runoff (∼40%) and water from the adjacent ophiolite aquifer (∼50%) (Table 8). The mixing fractions calculated for $\delta^{18}O$ and Cl agree with each other, and the observed composition and mineral saturation state of the target water can be reproduced by this mixture including dissolution of a magnesium carbonate phase in the alluvial sediments along flow path 3 (Table 8). Models including either dissolution of secondary dolomite (Model 1, Table 8) or magnesite (Model 2, Table 8) are in best agreement with the observed composition and mineral saturation state. But due to the very similar results between these two models and more or less similar $\delta^{13}C$ values of secondary dolomite (−6.9‰) and magnesite (−7.8‰), it is not possible to distinguish between these two magnesium carbonates as the dominant magnesium source.

The simulations can reproduce all measured concentrations of the target water with the exception of TIC (Table 8). This results in the inverse mass balance and mixing calculations in a mass transfer of $CO_2(g)$ into the aquifer ($CO_2$-ingassing), which is consistent with the less negative $\delta^{13}C_{TIC}$ value in the alluvial target water compared to the more negative $\delta^{13}C_{TIC}$ in the ophiolite water (−15.5‰) that makes up the dominant mixing fraction (Table 8). Furthermore, $CO_2(g)$ ingassing might occur along flow path 3, since the shallow aquifer in the piedmont area of Wadi Halfayn is unconfined and exchange with atmospheric $CO_2(g)$ seems to be possible.

**Table 7** Averaged chemical and isotopic composition of rainfall, surface water and groundwater from the piedmont area of Wadi Halfayn

| | Pure rain | Surface flow | Groundwater HSG low-altitude | Groundwater ophiolite | Target alluvial water |
|---|---|---|---|---|---|
| pH | 6.00 | 7.41 | 7.37 | 7.50 | 7.39 |
| $T$(°C) | 25.0 | 26.0 | 28.8 | 30.3 | 32.3 |
| Ca | 0.21 | 1.36 | 1.54 | 0.94 | 0.92 |
| Mg | 0.03 | 0.43 | 0.83 | 2.19 | 1.70 |
| Na | 0.06 | 0.62 | 1.25 | 2.17 | 1.40 |
| K | 0.02 | 0.05 | 0.05 | 0.05 | 0.06 |
| Si | na | 0.17 | 0.21 | 0.63 | 0.42 |
| $C_{TIC}$ | 0.02 | 3.36 | 3.40 | 4.34 | 4.44 |
| Cl | 0.08 | 0.63 | 1.33 | 2.06 | 1.44 |
| $SO_4$ | 0.04 | 0.16 | 0.53 | 0.60 | 0.36 |
| $NO_3$ | 0.09 | 0.02 | 0.05 | 0.09 | 0.16 |
| $\delta^{18}O$ (‰) | −1.67 | −2.26 | −2.59 | −0.97 | −1.68 |
| $\delta^{13}C$ (‰) | −7.00 | −6.32 | −7.20 | −15.50 | −12.45 |
| SI | | | | | |
| Calcite | | 0.00 | 0.00 | 0.00 | 0.00 |
| Dolomite | | −0.36 | −0.06 | 0.56 | 0.47 |
| Log $P_{CO_2}$ | −3.50 | −2.14 | −2.08 | −2.06 | −1.97 |
| Mg-calcite | | | | | 0.55 |
| Gypsum | | −2.46 | | −2.18 | −2.49 |
| Magnesite | | −0.94 | | | −0.12 |
| Brucite | | −4.58 | | | −4.49 |

The mean composition of rainfall and surface runoff were calculated using rainfall samples that were collected in the area during the period of 1997–1999 by the Ministry of Water Resources and the author (unpublished data). In addition, the average composition of ophiolite groundwater was calculated from samples, which originate from the ophiolite foothills east of flow path 3 (see Fig. 1). It includes sample 59 (Table 2) and six samples from Rathmayr (2000)

 DOI 10.1007/s10040-004-0425-2

**Table 8** Results of the chemical and isotope mass balance calculations including mixing to evaluate the potential recharge and magnesium sources for the alluvial groundwater in the piedmont of Wadi Halfayn. Model 1 includes secondary dolomite and Model 2 magnesite as possible magnesium sources. Positive numbers in the mass transfer indicate dissolution of the mineral phase and negative number precipitation. The simulated chemical composition is compared to the observed one (target alluvial water, cf. Table 7)

| | Simulated chemical composition and saturation states | | Target alluvial water (measured) |
|---|---|---|---|
| pH | 7.44 | 7.43 | 7.39 |
| Ca | 1 | 1.02 | 0.92 |
| Mg | 1.69 | 1.69 | 1.7 |
| Na | 1.39 | 1.38 | 1.4 |
| $C_{TIC}$ | 4.31 | 4.36 | 4.44 |
| Cl | 1.35 | 1.33 | 1.44 |
| $SO_4$ | 0.38 | 0.38 | 0.36 |
| Saturation indices | | | |
| Calcite | 0 | 0 | 0 |
| Dolomite | 0.4 | 0.38 | 0.42 |
| $pCO_2$ | −2.05 | −2.03 | −1.92 |
| Magnesite | −0.19 | −0.2 | −0.15 |
| Gypsum | −2.31 | −2.3 | −2.5 |
| Mixing calculations | Model 1 | Model 2 | |
| Mixing fractions | | | |
| Rain | 0.089 | 0.1085 | |
| Surface flow | 0.38 | 0.3609 | |
| Ophiolite water | 0.5266 | 0.5306 | |
| Mass transfer (mmol/kg $H_2O$) | | | |
| Phases | | | |
| Calcite | −0.42 | | |
| Secondary dolomite | 0.37 | | |
| Magnesite | | 0.37 | |
| $CO_2$(g) | 0.39 | 0.46 | |

### *Southern alluvial plain aquifer*

South of the piedmont area groundwater from Wadi Abydah (flow path 1) and Wadi Mu'aydin (flow path 2) mixes and merges with groundwater from Wadi Halfayn (flow path 3) and flows southwards towards the Adam Mountains. Southern Alluvial Plain groundwaters display a similar mineral saturation as calculated for the alluvial piedmont groundwaters except that they become less undersaturated with respect to gypsum (Table 4) as a function of distance. It should be recalled here that the alluvial deposits of the Southern Alluvial Plain consist of about equal amounts of Hajar Supergroup carbonate and weathered ophiolitic (containing brucite and magnesite) debris. In addition, gypsum and halite are observed in salt crusts at the surface and in near-surface levels where they are formed during evaporation of water derived from weak precipitation or wadi flood events. The alluvial deposits are cemented to different degrees with secondary disordered dolomite, calcite and high-magnesium calcite (HMC).

Mixing of two (or more) water components might result in additional mineral dissolution even when the individual components are in equilibrium with respect to that mineral phase, given that there are significant enough differences in the chemistry of the two components (e.g. Plummer 1975; Appelo and Postma 1996). Mixing calculations show that the chemical compositions of the alluvial piedmont groundwaters are too similar to induce significant additional mineral dissolution. Therefore, mixing cannot explain the increase in Cl, Na, $SO_4$, Ca and Mg observed in the Southern Alluvial Plain groundwaters from north to south. As shown in Figs. 8 and 9 this general increase with distance is interrupted by segments with lower concentrations between sample location 49 and 52 and 53–55 (cf. Fig. 1), indicating a larger contribution of more dilute water from Wadi Halfayn (flow path 3) and the Bahla System, respectively (Fig. 1). In spite of the above-mentioned segmentation the general trend of groundwater evolution remains unchanged.

Because mixing of piedmont groundwaters cannot explain the observed increase in solutes, there must be a driving force for additional mineral dissolution along the flow path from north to south in the Southern Alluvial Plain. As

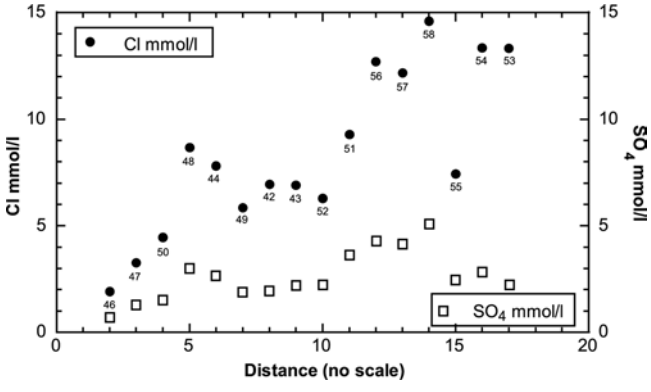


**Fig. 8** Cl and $SO_4$ vs. distance plot of groundwater samples along the N–S flow path in the Southern Alluvial Plain shows the general trend to higher concentrations further down gradient. Note the interruption of the general trend (see text for explanation)

 DOI 10.1007/s10040-004-0425-2

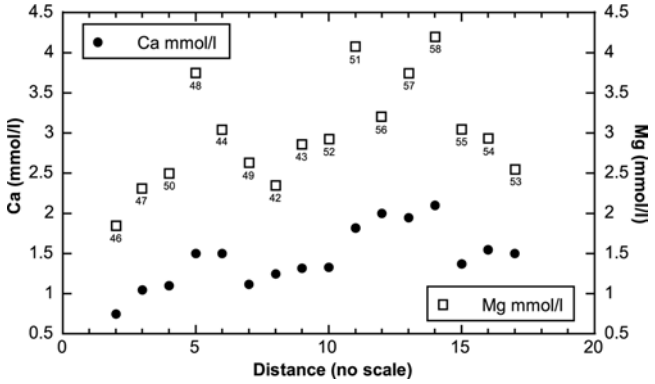


**Fig. 9** Ca and Mg vs. distance plot of groundwater samples along the N–S flow path in the Southern Alluvial plain illustrates the general trend of increasing concentrations along the flow path. The increase is not linear with distance. Note the interruption of the general trend between sample locations 49–52 and 53–55 (see text for explanation)

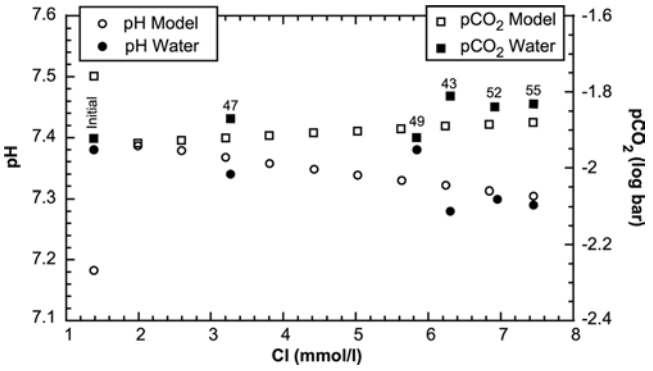


**Fig. 10** Comparison of modeled and measured pH and $pCO_2$ during dedolomitization as a function of the reaction progress

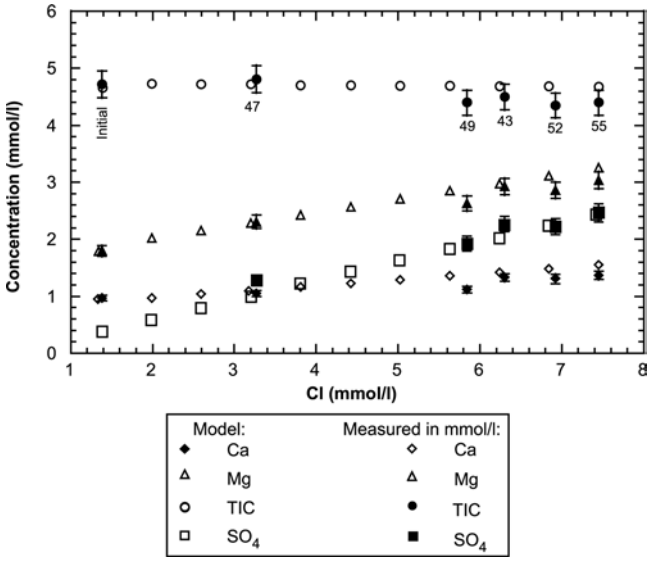


**Fig. 11** Comparison of modeled and measured calcium, magnesium, total inorganic carbon and sulfate concentrations during dedolomitization as a function of the reaction progress here represented by the increase in Cl

shown in Fig. 6, the concentrations of Mg and Ca correlate with that of sulfate. This suggests that dedolomitization, i.e. dolomite dissolution induced by the dissolution of gypsum while maintaining equilibrium with calcite (e.g. Back et al. 1983; Plummer et al. 1990), might be the responsible process. Dissolution of other minerals in the alluvial gravels such as brucite, serpentine, magnesite, and primary ophiolite minerals may explain the increase in Mg concentrations, but it cannot explain those of $SO_4$ and Ca. In addition, dissolution of the primary ophiolite minerals cannot account for the almost constant Si concentration, and moreover they have also slower dissolution kinetics compared to dolomite (e.g. Chou et al. 1989; Brantley and Chen 1995). Although dissolution of such minerals might still occur to some degree, it does not explain the overall geochemical evolution of the Southern Alluvial Plain groundwaters.

To test the proposed hypothesis of dedolomitization as the dominant evolutionary process of the Southern Alluvial Plain groundwaters, reaction path calculations were performed using the Cl concentration as a reaction progress variable. An average alluvial piedmont groundwater (target alluvial water in Table 5) was taken as starting solution whereas an evolved groundwater from the Southern Alluvial Plain (AG35, sample location 55, see Table 2 and Fig. 1) was adopted as final solution to calculate the difference in Cl concentration. In fact, the dedolomitization model can predict within the cumulative error the compositional changes and saturation states of groundwaters as observed from north to south in the Southern Alluvial Plain (Figs. 10–12). Using one of the above alternative sources for Mg combined with gypsum dissolution, however, the model calculations cannot predict the observed concentrations of Mg and Ca (magnesite) and the pH and $pCO_2$ (brucite, primary ophiolite minerals). Similarly, the model using high-magnesium calcite, for which an equilibrium constant was calculated for a solid-solution with 30 mol% Mg according to Busenberg and Plummer (1989), does not predict the Ca and Mg concentrations and pH within the cumulative error.

However, there is only fair agreement between modeled and observed $\delta^{13}C_{TIC}$ values and the dedolomitization model yields too low $^{14}C$ activities compared to the measured ones (Fig. 13). For the $\delta^{13}C_{TIC}$ one might argue that the assumed average values for secondary carbonate cements ($\delta^{13}C = -8.5‰$PDB) might not be entirely representative. Furthermore, possible effects on the carbon isotope composition during mixing with lower mineralized groundwater from flow path 3, as suggested from the Cl and $SO_4$ concentrations (Fig. 8), are not taken into account by the calculations. Unfortunately, the lack of $\delta^{13}C$ data from the cements in the Southern Alluvial Plain and the large spread observed in isotopic data of such cements (Burns and Matter 1995) do not allow better constraint of the calculations.

In the model, the $^{14}C$ activity drops rapidly from the assumed starting value (100 pmc) to values between 60 and 70 pmc and then continuously to values below 40 pmc (Fig. 13). The initial rapid drop is due to the large amount of $^{14}C$-free carbonate from the induced dolomite dissolu-

 DOI 10.1007/s10040-004-0425-2

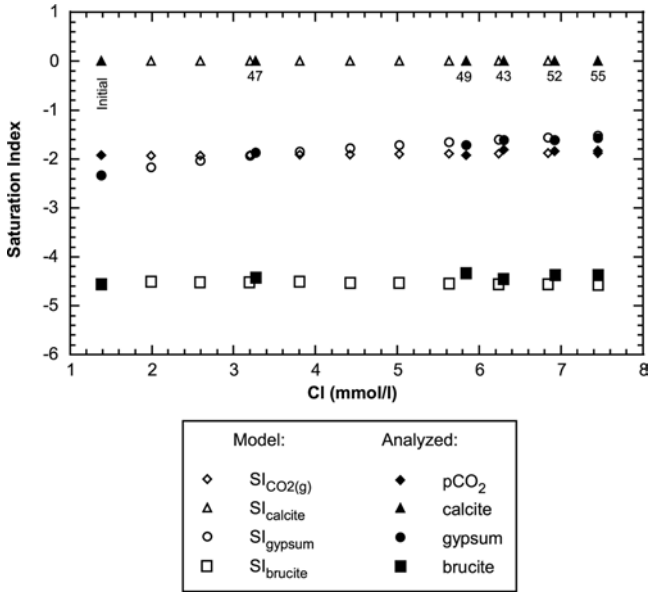


**Fig. 12** Modeled mineral saturation indices and $pCO_2$ as a function of the reaction progress compared with those calculated for the individual measured groundwater compositions along the flow path

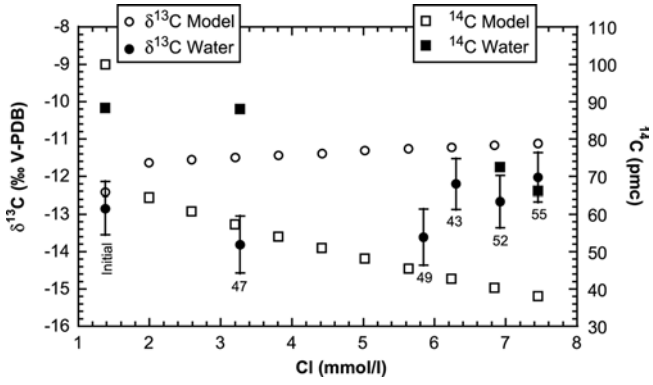


**Fig. 13** Comparison of modeled and measured $\delta^{13}$C-values and $^{14}$C activities during dedolomitization. Error bars for $^{14}$C measurements have the same size as the symbols and are not plotted

tion, which gradually decreases as soon as dolomite approaches equilibrium. Sensitivity analysis shows that the calculated $^{14}$C activities are sensitive to the assumed starting value at the beginning of the proposed evolutionary path but no more towards its end. This strongly suggests that in the southern alluvium a local modern component high in $^{14}$C must mix with the groundwater derived from the piedmont. It should be noted that direct infiltration into the southern alluvium could be either rainfall and/or surface runoff in the wadi channels as a result of strong rain events. Such infiltration would result in a similar chemical composition because the rain/surface water would react with the salt and gypsum crust and the same alluvial sediments during its infiltration as does the groundwater. This even allows a rough estimate of this locally infiltrated component, which is in the order of 40–50% for the last two sampling locations (52 and 55) based on $^{14}$C. Obviously, this estimate has to be treated carefully and needs to be supported by other isotopic data for which, however,

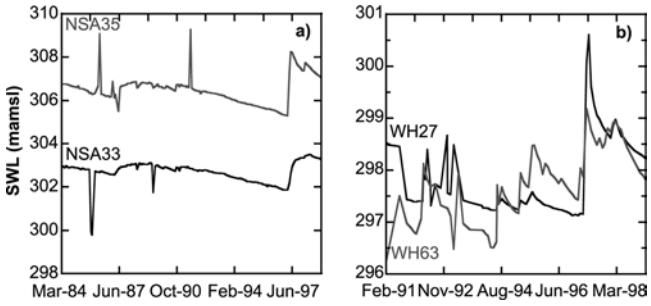


**Fig. 14** (**a**) Pressure response (hydrograph) in two wells from the deep alluvial aquifer (interfluvial area), and (**b**) pressure response of two wells from the shallow alluvial aquifer along active wadi channels. All four wells are situated in the southern alluvial plain and their pressure response illustrates differences in recharge frequency (see Table 2 for locations)

monitoring of groundwater over a longer time period is required.

Local infiltration proposed on the $^{14}$C data in the Southern Alluvial Plain does not contradict the low $^{3}$H activities observed in some of the deep groundwaters such as at locations 52 and 55. Hydrograph measurements show distinct differences in recharge frequency between deep and shallow wells, the latter being situated in active wadi channels. As shown in Fig. 14, the $^{3}$H-free deep groundwater at locations 52 an 55 (wells NSA35A and AG35) display an irregular recharge frequency between about every 4–6 years, while a more regular, almost annual frequency is observed for $^{3}$H-bearing shallow wells (e.g. location 57). This suggests that in the deeper alluvial aquifer the $^{3}$H activity of the locally infiltrated water component might decrease considerably, while the $^{14}$C activity only imperceptibly changes between two infrequent local recharge events. Large differences in $^{3}$H activity between shallow and deep alluvial groundwaters were also observed by Cansult/Gartner and Lee (1986) and Clark (1987). These authors proposed that the shallow alluvial groundwater in the Southern Alluvial Plain that has been recharged by wadi flow originating in the Jabal Akhdar exhibits ages between 5 and 10 years. In contrast, the average residence time of groundwater sampled away from active wadi channels in the Southern Alluvial Plain is older than about 35 years.

### *Adam Mountains*

The highly mineralized deep groundwaters of the from Hajar Supergroup aquifer of the Adam Mountains display the same mineral saturation state as those from the Hajar Supergroup aquifer from the Jabal Akhdar, except that they are also in equilibrium with chalcedony ( $SI = 0 \pm 0.1$). Their chemical composition indicates an advanced state of groundwater evolution, which, however, cannot be entirely resolved based on the present data. The absence of measurable $^{3}$H indicates for the $\delta^{13}C_{TIC}$ values ($-6.7$ to $-10.6$‰) of these groundwaters that the dissolved carbon might partly come from marine sediments (less negative values). In addition $\delta^{13}C_{TIC}$ values are influenced by sulfate reduction as observed in the Adam Mountains groundwaters. Adopting a similar chemical evolution as for

 DOI 10.1007/s10040-004-0425-2

the southern alluvial groundwater, a corrected maximum $^{14}C$ residence time of more than 3,500 years is calculated for location 69 (well ADM03 in Tables 2–4). Although the stable water isotopes might indicate a predominantly southern moisture source for these waters under present-day conditions (Fig. 7), such an interpretation has to be treated carefully because of the large uncertainty attached to the backwards extrapolation of present-day precipitation isotopic data over several thousands of years.

## Conclusions

Geochemical modeling in combination with environmental isotope data led to the following qualitative and quantitative assessment of the origin and geochemical evolution of the different groundwater types in the Halfayn alluvial aquifer system:

A. Piedmont alluvial groundwaters along flow path 1 (Wadi Abyadh) and 2 (Wadi M'uaydin) represent a mixture between high-altitude water derived from the Hajar Supergroup aquifer of the Jabal Akhdar and locally infiltrated water. This latter component is significant as indicated by the higher $^{3}H$ and $^{14}C$ activities, the less depleted $^{18}O$ values, and more negative $\delta^{13}C_{TIC}$ values, which are derived from secondary carbonate dissolution. The unevenly timed recharge events, however, result in a rather large spread in chemical and isotopic compositions, which inhibits a quantification of the individual proportions based on a single data set.
B. The chemical and isotopic composition of groundwater along flow path 3 (Wadi Halfayn) is the result of a three component mixture of water originating from the Jabal Akhdar as surface runoff, the ophiolite aquifer and local recharge by infiltrating rain water, whereas significant inflow (~50%) is provided from the adjacent ophiolite foothills as lateral recharge through surface runoff or subsurface inflow. This results in characteristically increased Mg/Ca ratios, increased chloride concentrations, and less depleted $\delta^{18}O$ values similar to those from the ophiolite aquifer.
C. Direct infiltration by either rainfall and/or surface runoff in the wadi channels was found to be an important source of recharge to the alluvial aquifer in the Southern Alluvial Plain. The combination of chemical and (radio)isotope data revealed that the observed groundwater compositions can only be explained by a mixture between this modern direct infiltration component and groundwater derived from the piedmont with a longer residence time. The geochemical evolution is characterized by dedolomitization as the main process besides halite dissolution as can be shown by reaction path modeling and which is consistent with the (hydro)geologic observations.
D. When compared to existing local meteoric water lines of Oman, the groundwater stable isotope data ($^{18}O$, $^{2}H$) from the different aquifers from the study area suggest that different moisture sources contribute to recharge. Groundwater from the Hajar Supergroup aquifer of the Jabal Akhdar is a mixture between a typical northern and southern moisture source. A significant northern moisture source is also present in the piedmont alluvial groundwaters. In contrast, the stable isotope composition of groundwaters from the ophiolite aquifer, the alluvial aquifer in the Southern Alluvial Plain and the Hajar Supergroup aquifer of the Adam Mountains indicates that recharge occurs predominantly from southern moisture sources (low-pressure systems and/or tropical cyclones).

Overall, this study provides new detailed information about different recharge areas, sources of recharge and the geochemical evolution of groundwater in the Halfayn alluvial aquifer system. In addition, the combination of isotopic with geochemical data and the integration of these data in a regional hydrogeochemical model allowed to set new boundary conditions for the alluvial aquifer and improve the understanding of a complex aquifer system in an arid area.

**Acknowledgments** We thank the Ministry of Regional Municipalities Environment and Water Resources in the Sultanate of Oman for their permission to do this field work, for their logistic and scientific support and for the chemical analyses of all water samples. We are deeply grateful to Zaher Al Suleimani, Director General of Groundwater Resources, Ahmed Al Malki, Acting Director of Research and Suleiman Al Abri, former Director of the Ministry of Water Resources Regional Office Nizwa for their assistance during this project. We also thank several people, namely Hashim Al Balushi, Salim Al Ma'shari and Sidney Da Silva from the Ministry of Water Resources for their assistance in the field. The authors are grateful to Phil Macumber and an anonymous reviewer for the constructive reviews

## References

Adar EM, Neuman SP (1988) Estimation of spatial recharge distribution using environmental isotopes and hydrochemical data, II. Application to Aravaipa Valley in southern Arizona, USA. J Hydrol 97:279–302

Appelo CAJ, Postma D (1996) Geochemistry, groundwater and pollution, 3rd edn. Balkema, Rotterdam

Atkins WS (1986) Hydrogeology and water resources of the Greater Manah area. Study Report, Ministry of Water Resources, Sultanate of Oman

Back W, Hanshaw BB, Plummer LN, Rahn PH, Rightmire CT, Meyer R (1983) Process and rate of dedolomitization: mass transfer and $^{14}C$ dating in a regional carbonate aquifer. Geolo Soc Am Bull 94:1415–1429

Ball JW, Nordstrom DK (1991) User's manual for WATEQ4F, with revised thermodynamic data base and test cases for calculating speciation of major, trace, and redox elements in natural waters. U.S. Geological Survey, Reston, VA, USA

Berner RA (1975) The role of magnesium in the crystal growth of calcite and aragonite from sea water. Geochim Cosmochim Acta 39:489–504

Brantley SL, Chen Y (1995) Chemical weathering rates of pyroxenes and amphiboles. In: White AF, Brantley SL (eds) Chemical weathering of silicate minerals. American Mineral Society. Washington, DC, USA. Rev Mineral 31:119–172

Burns SJ, Matter A (1995) Geochemistry of carbonate cements in surficial alluvial conglomerates and their paleoclimatic implications, Sultanate of Oman. J Sedimen Res A65(1):170–177

 DOI 10.1007/s10040-004-0425-2

Busenberg E, Plummer LN (1982) The kinetics of dissolution of dolomite in $CO_2$–$H_2O$ systems at 1.5 to 65°C and 0 to 1 atm . Am J Sci 282:45–78

Busenberg E, Plummer LN (1989) Thermodynamics of magnesian calcite solid-solution at 25 degrees C and 1 atm total pressure. Geochim Cosmochim Acta 53(6):1189–1208

Cansult/Gartner and Lee (1986) Origin and age of groundwater in Oman. A study of environmental isotopes. PAWR Report 86/7, Sultanate of Oman

Chou L, Garrels RM, Wollast R (1989) Comparitive study of the kinetics and mechanisms of dissolution of carbonate minerals. Chem Geol 78:269–282

Clark ID (1987) Groundwater Resources in the Sultanate of Oman: origin, circulation times, recharge processes and paleoclimatology. Isotopic and geochemical approaches. PhD Thesis, Université de Paris-Sud, Centres d'Orsay, France

Clark ID, Fritz PE (1997) Environmental isotopes in hydrogeology, 1st edn. CRC Press, Boca Raton

Clark ID, Fontes JC (1990) Paleoclimatic reconstructions in Northern Oman based on carbonates from hyperalkaline groundwaters. Quat Res 33:320–336

Clark ID, Fritz P, Quinn OP, Rippon PW, Nash H, Bin Ghalib Sayyid Barghash, Al Said (1987) Modern and fossil groundwater in an arid environment: A look at the hydrogeology of Oman. In: Isotope techniques in water resources development. International Atomic Energy Agency, Vienna, pp 167–187

Edmunds WM, Walton NRG (1980) A geochemical and isotopic approach to recharge evalution in semi-arid zones; past and present. In: Fontes JC (ed) Arid-zone hydrology, investigation with isotope techniques. International Atomic Energy Agency, Vienna, pp 47–68

Edmunds WM, Gaye CB (1994) Estimating the spatial variability of groundwater recharge in the Sahel using chloride. J Hydrol 156:47–59

Gibb A, Partner (1976) Water Resources Survey of Northern Oman. Report Directorate General of Finance, Sultanate of Oman

Glennie KW, Boeuf MGA, Hughes Clarke MW, Moody-Stuart M, Pilaar WFH, Reinhardt BME (1974) Geology of the Oman mountains. Verh Kon Ned Geol Minjnb Gen, Delft, Netherlands

Gonfiantini R (1978) Standards for stable isotope measurements in natural compounds. Nature 271:534–536

Hoefs J (1997) Stable isotope geochemistry. Springer, Berlin, New York

Issar A, Nativ R, Karnieli A, Gat JR (1983) Isotopic evidence of the origin of groundwater in arid zones. In: Anon. Isotope hydrology. International Atomic Energy Agency, Vienna

Lippard SJ, Shelton AW, Gass IE (eds) (1986) The Ophiolite of Northern Oman. Geological Society of London Memoir No. 11

MacDonald M (1994) Adam water supply. Borehole Drilling and Testing Report, Ministry of Water Resources, Sultante of Oman

MacDonald M (1982) Saiq water supply study. Report, Ministry of Water Resources, Sultanate of Oman

Macumber PG (2003) Lenses, plumes and wedges in the Sultanate of Oman: a challenge for groundwater management. In: Alsharhan AS, Wood WW (eds) Water resources perspectives: evaluation, management and policy. Elsevier Science, Amsterdam, The Netherlands, pp 349–370

Macumber PG (1998) The Cable Tool program and groundwater flow in the Eastern Batinah alluvial aquifer. Report of Directorate of Water Resources Assessment, Ministry of Water Resources, Sultanate of Oman, pp 159

Macumber PG (1997) Al Khawd Fan groundwater investigation. Final report, Directorate General of Water Resources Assessment, Ministry of Water Resources, Sultanate of Oman, pp 65

Macumber PG (1995) Freshwater lenses in the hyper-arid region of Central Oman. In: International Conference on Water Management in Arid Countries, Muscat, March 1995, pp 480–487

Macumber PG, Niwas JM, Al Abadi A, Seneviratne R (1997) A new isotopic water line for northern Oman. In: Proceedings of the Third Gulf Water Conference, Muscat 1997, pp 141–162

Macumber PG, Bin Ghalib Sayyid Barghash, Kew GA, Tennakoon TB (1995) Hydrogeologic implications of a cyclonic rainfall event in central Oman. In: Nash H, McCall GJH (eds) Groundwater quality. Chapman and Hall, London, pp 87–97

Matter JM (2001) Geochemical evolution and hydrodynamics of groundwaters in the Alluvial Aquifer of the Dakhiliya Area, Sultanate of Oman. PhD Thesis, Swiss Federal Institute of Technology Zurich, Switzerland

MWR (1994) Wadi Samail detailed resource assessment. Water Resources Assessment Report, Ministry of Water Resources, Sultanate of Oman

MWR (1995) Data Compilation and Review: Dakhliya Region. Report, Ministry of Water Resources, Sultanate of Oman

MWR (1996) Jabal Akhdar Hydrogeological Assessment. Water Resources Assessment Report, Ministry of Water Resources, Sultanate of Oman

Nativ R, Dahan O, Nissim I, Adar EM, Geyh ME (1995) Questions pertaining to isotopic and hydrochemical evidence of fracture-controlled water flow and solute transport in a chalk aquitard. In: Adar EM, Leibundgut C (eds) Application of tracers in arid hydrology. IAHS Press, Wallingford, UK, pp 317–327

Neal C, Stanger G (1985) Past and present serpentinisation of ultramafic rocks; an example from the Semail Ophiolite nappe of northern Oman. In: Drever JI (ed) The chemistry of weathering. NATO ASI Series, Series C, D. Reidel Publishing Company, Dordrecht-Boston, pp 249–275

Pallister JS, Hopson CA (1981) Samail ophiolite plutonic suite: field relations, phase variation, cryptic variation and layering and a model of a spreading ridge magma chamber. J Geophys Res 86(B4):2593–2644

Parkhurst DL, Appelo CAJ (1999) User's guide to PHREEQC (version 2)—a computer program for speciation, batch-reaction, one-dimensional transport, and inverse geochemical calculations. U.S. Geological Survey Water-Resources Investigations Report 99-4259

Pearson FJ Jr, Fisher DW, Plummer LW (1978) Correction of ground-water chemistry and carbon isotopic composition for effects of $CO_2$ outgassing. Geochim Cosmochim Acta 42:1799–1807

Peters T, Nicolas A, Coleman RGE (eds) (1990) Ophiolite genesis and evolution of the oceanic lithosphere, series: petrology and structural geology vol 5. In: Conference Proceedings of the Ophiolite Conference. Kluwer Academic Publishers, Dordrecht

Plummer LN (1975) Mixing of sea water with calcium carbonate groundwater. Memoire Geolog Soc Am 142:219–236

Plummer LN, Parkhurst DL, Wigley TML (1979) Critical review of the kinetics of calcite dissolution and precipitation. In: Jenne EA (ed) Chemical modeling in aqueous systems. Am Chem Soc Symp Ser 93:537–573

Plummer LN, Busby JF, Roger WL, Hanshaw BB (1990) Geochemical modeling of the Madison aquifer in parts of Montana, Wyoming, and South Dakota. Water Resour Res 26(9):1981–2014

Plummer LN, Prestemon EC, Parkhurst DL (1994) An interactive code (NETPATH) for modeling net geochemical reactions along a flow path, version 2.0. U.S. Geological Survey Water Resources Investigations Report, pp 94–4169

Rabu D, Le-Metour J, Béchennec F, Beurrier M, Villey M, Bourdillon-Jeudy de Grissac C (1990) Sedimentary aspects of the Eo-Alpine cycle on the northeastern edge of the Arabian Platform (Oman Mountains). In: Robertson AHF, Searle MP, Ries AC (eds) The geology and tectonics of the Oman region. Geol Soc London Special Publ 49:49–68

Rathmayr B (2000) Geology and hydrogeology of the Birkat al Mawz-Izki Area (Sultanate of Oman). MS Thesis, University of Bern, Switzerland

Rimstidt JD (1997) Quartz solubility at low temperatures. Geochim Cosmochim Acta 61(13):2553–2558

Robertson AHF, Searle MP, Ries AC (eds) (1990) The geology and tectonics of the Oman region. Geol Soc London Special Publ 49

Rozanski K, Araguás-Araguás LE (1992) Statistical treatment of data on environmental isotopes in precipitation. Int Atomic Energy Agency Tech Rep Ser :pp 331

Simmers I (ed) (1997) Recharge of Phreatic aquifers in (semi-) arid areas, International Association of Hydrogeologists, vol 19. Balkema, Rotterdam

Stalder PJ (1975) Cementation of Pliocene-Quaternary fluviatile clastic deposits in and along the Oman Mountains. Geologie en Mijnbouw 54(3–4):148–156

Stanger G (1986) The hydrogeology of the Oman Mountains. PhD Thesis, Open University London, UK

Swart PK, Burns SJ, Leder JJ (1991) Fractionation of the stable isotopes of oxygen and carbon in carbon dioxide during the reaction of calcite with phosphoric acid as a function of temperature. Chem Geol 86:89–96

Taylor D, Jones PD, Wigley TML (1990) Rainfall in Oman: data acquisition, statistics and climatology. Report Ministry of Water Resources, Muscat, Oman

Weyhenmeyer C (2000) Origin and evolution of groundwaters in the alluvial aquifer of the Eastern Batinah Coastal Plain, Sultanate of Oman. PhD Thesis, University of Bern, Switzerland

Weyhenmeyer C, Burns SJ, Waber HN, Macumber PG, Matter A (2002) Isotope study of moisture sources, recharge area, and groundwater flow paths within the eastern Batinah coastal plain, Sultanate of Oman. Water Resour Res 38(10):2-1–2-22

Wushiki H (1991) $^{18}O/^{16}O$ and D/H of the meteoric waters in South Arabia. Mass Spectrom 39(5):239–250

 DOI 10.1007/s10040-004-0425-2